



2013

Background Paper Prepared for the Global Assessment Report on  
Disaster Risk Reduction 2013

**Landslide Hazard and Risk Assessment in El Salvador**

**Norwegian Geotechnical Institute (NGI)**



Geneva, Switzerland, 2013

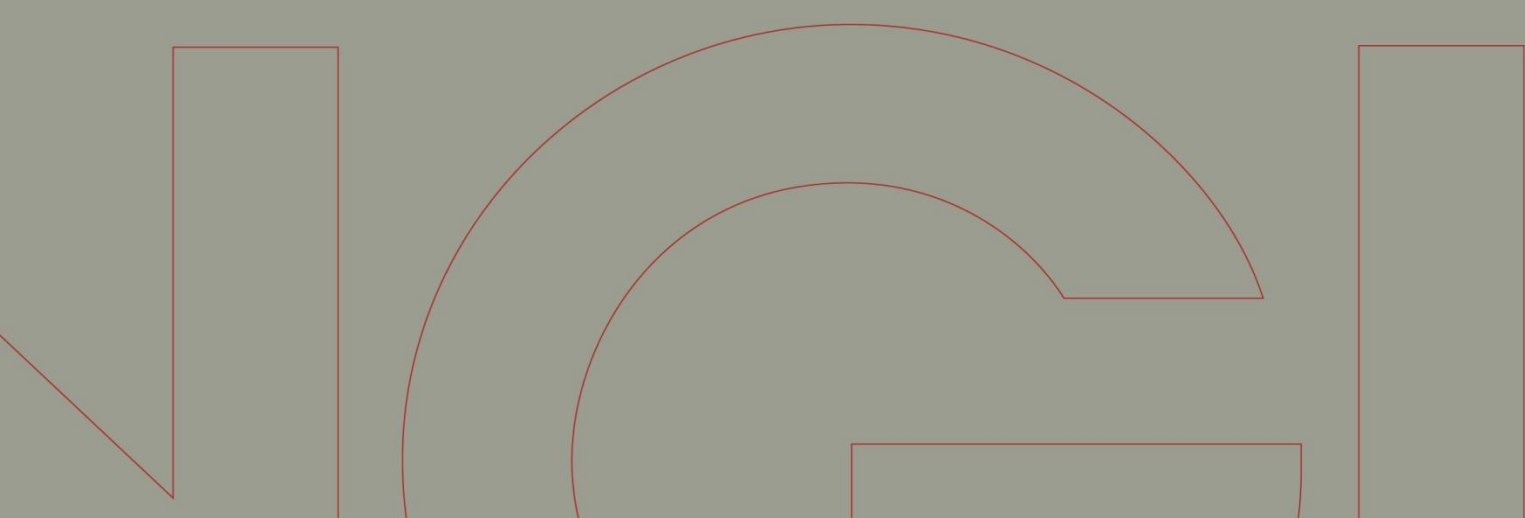


Rapport / Report

# UNISDR Global Assessment Report 2013 - GAR13

## Landslide Hazard and Risk Assessment in El Salvador

20120052-01-R  
14 December 2012  
Revision: 0



Ved elektronisk overføring kan ikke konfidensialiteten eller autentisiteten av dette dokumentet garanteres. Adressaten bør vurdere denne risikoen og ta fullt ansvar for bruk av dette dokumentet.

Dokumentet skal ikke benyttes i utdrag eller til andre formål enn det dokumentet omhandler. Dokumentet må ikke reproduseres eller leveres til tredjemann uten eiers samtykke. Dokumentet må ikke endres uten samtykke fra NGL.

Neither the confidentiality nor the integrity of this document can be guaranteed following electronic transmission. The addressee should consider this risk and take full responsibility for use of this document.

This document shall not be used in parts, or for other purposes than the document was prepared for. The document shall not be copied, in parts or in whole, or be given to a third party without the owner's consent. No changes to the document shall be made without consent from NGL.



## Project

Project title: UNISDR Global Assessment Report 2013  
- GAR13  
Document title: Landslide Hazard and Risk Assessment in  
El Salvador  
Document No.: 20120052-01-R  
Date: 14 December 2012  
Revision/Rev. date: 0

Main office:  
PO Box 3930 Ullevål Stadion  
NO-0806 Oslo  
Norway

Trondheim office:  
PO Box 1230 Sluppen  
NO-7462 Trondheim  
Norway

T (+47) 22 02 30 00  
F (+47) 22 23 04 48

BIC No. DNBANOKK  
IBAN NO26 5096 0501 281  
Company No.  
958 254 318 MVA

[ngi@ngi.no](mailto:ngi@ngi.no)  
[www.ngi.no](http://www.ngi.no)

## Client

Client: The United Nations Office for Disaster  
Risk Reduction – UNISDR  
Client's contact person: Andrew Maskrey  
Contract reference: Signed agreement dated 16 November  
2012

## For NGI

Project manager: Farrokh Nadim  
Prepared by: José Cepeda and Barbara Schwendtner  
Contributions also from: Byron Quan Luna (NGI),  
Manuel Díaz and Giovanni Molina  
(Dirección General del Observatorio  
Ambiental –DGOA-, Ministry of  
Environment and Natural Resources of El  
Salvador)  
Reviewed by: Farrokh Nadim

## Summary

Landslides in El Salvador constitute an important natural hazard due to prevailing steep terrain covered with unconsolidated volcanic sediments and the frequent occurrence of extreme precipitation events and intense earthquakes. These high landslide hazard conditions occur in a country with the highest population density in the mainland Americas. Worldwide, among countries and territories with more

# Summary (cont.)



Document No. : 20120052-01-R  
Date: 2012-12-14  
Revision.: 0  
Page: 5

than 5 million habitants, there are only 14 countries with a higher population density than El Salvador.

The two earthquakes in January and February 2001 caused more than 1000 casualties, 90% of whom were due to co-seismic landslides, most of them in one single event in a neighbourhood of the municipality of Santa Tecla. In November 2009, the tropical storm “Ida” delivered in only 5 hours more than 5 times the mean monthly precipitation in the San Vicente volcano, triggering numerous landslides that travelled more than 6 km from the source and killed almost 200 people.

The aforementioned facts combined with results from global risk evaluations, indicate that El Salvador is among the countries where drill-down studies are relevant for advancing the knowledge on landslide hazard and investigating the connections between the consequences on population and human development. For the present study, country-wide, event-based landslide inventories were available for events triggered during Hurricane Mitch in 1998 and during the two earthquakes in January and February 2001. These inventories were prepared by mapping events using remote sensing techniques. In addition, national authorities supplied an inventory of landslides mostly reported due to their consequences in inhabited areas or roads.

The present hazard assessment employed three different methods: the heuristic model used previously in the GAR 2009 and 2011 assessments, the bivariate method, and the weights of evidence method. These last two methods have a statistical basis that requires calibration from correlation with known incidents. Therefore, the methods were feasible and suitable for the present evaluation considering the availability of inventories. A single hazard map was obtained for each triggering condition (rainfall and earthquake) from a weighted sum of the results of the three models.

The common spatial datasets for the two types of hazard evaluation were a 10-m digital elevation model, a 1:100 000 geologic map, a land cover map, and aggregated monthly precipitation over the rainy season, which was used as a proxy for soil moisture. The following sub-products of the digital elevation model were used to characterize topographic conditions: slope angle, elevation, aspect, planar curvature, and profile curvature. A heuristic classification of the geologic and land cover maps was performed in consultation with local experts. The triggering factor for earthquake conditions was provided from a recent probabilistic hazard assessment in terms of horizontal peak ground acceleration. The calibration of the susceptibility and triggering factors was performed with a numerical simulation of ground accelerations associated to the seismic sources of the 2001 earthquakes and the corresponding event-based inventory of landslides. In a similar manner, the calibration for hazard due to rainfall-induced landslides used the precipitation conditions during Hurricane Mitch and a landslide inventory mapped from the pre- and post-Mitch aerial photos. The rainfall triggering factor was obtained from a spatial interpolation of point estimates of extreme rainfall using a country-wide network of 287 rain gauges.

# Summary (cont.)



Document No. : 20120052-01-R  
Date: 2012-12-14  
Revision.: 0  
Page: 6

The resulting hazard maps indicate much lower hazard due to earthquake-induced events than to rainfall-induced landslides in the northern part of the country. This difference is explained by the fact that seismic hazard is considerably higher on the south and central part of the country compared with the northern part. This is due to the proximity to the subduction zone to the south of the country and local systems of faults that run along the centre of the territory from west to east. These differences in seismicity control the spatial variation in landslide hazard when comparing the two types of triggering conditions.

Most of the country's population is settled in the three largest cities that lie along the central valleys that run from West to East. They are flanked by an active volcanic chain, which is in an ongoing mass wasting process in form of erosion and landslides due to the steep slopes and loose surface deposits. In particular, the Metropolitan Area of San Salvador, located at the centre of the country, concentrates about one third of the total population of 6 million.

In El Salvador, human development seems to be strongly correlated to the urban or rural nature of the settlements. The large urban centres in Santa Ana, San Salvador and San Miguel represent municipalities with high Human Development Index, HDI, which reaches a maximum of 0.88 in Antiguo Cuscatlán, one of the municipalities of the Metropolitan Area of San Salvador. The municipalities with the lowest HDI are mostly located to the north of the country, where rural settlements are abundant in areas that were strongly affected by a 12-year Civil war that ended two decades ago. The minimum HDI in the country is 0.56. Most of the municipalities with the lowest HDI are in the Departments of Morazán and Cabañas.

Population exposure was evaluated using the hazard maps for both types of triggering factors and the map of population density. The main difference is the lower exposure along the north of the country for earthquake-induced conditions than the corresponding to rainfall-triggered landslides. This is an obvious consequence of the differences in hazard distribution previously explained.

Risk for precipitation-induced landslides was calibrated at municipal level using the corresponding exposure values, data from DesInventar (for estimating consequences), and Human Development Index (HDI). Consequences data were available for 76 of the 262 municipalities.

The calibration explained about 36% of the variation of the risk data, which indicates a low correlation. The correlation of each predictor with risk was as follows (the sign indicates whether the correlation is direct, "+" sign, or inverse, "-" sign):

- Physical exposure (+)
- Human Development Index (HDI) (+)

## Summary (cont.)



Document No. : 20120052-01-R  
Date: 2012-12-14  
Revision.: 0  
Page: 7

Hence, an increase in physical exposure and in Human Development Index leads to an increase in risk. For Human Development Index, this is unexpected since an improvement in the mean development level in an area (increase in HDI) normally should reduce the risk. In the case of El Salvador, this unexpected correlation between risk and HDI is, however, confirmed by historical observations. In September 1982, a single rainfall-induced debris flow initiated in the San Salvador volcano and caused 500 casualties in a neighbourhood in the municipality of Mejicanos, which has the 4<sup>th</sup> highest HDI in the country (0.826). This positive correlation between HDI and mortality risk was also obtained in Nepal and Sri Lanka in a previous assessment performed by NGI in South Asia. A possible explanation of this positive correlation is that all these countries (El Salvador, Nepal and Sri Lanka) experienced civil conflict in recent decades, which led to rapid, uncontrolled migration of people from rural to urban centres and taking up residence in hazardous areas.

The calibrated equation of landslide risk in El Salvador is as follows:

$$\ln R_r = -5.48 + 0.206 \ln PE_r + 7.983 \ln \left( \frac{HDI_{SN}}{HDI_N} \right)$$

where  $R_r$  is the mortality risk (fatalities per year) due to precipitation-induced landslides,  $PE_r$  is physical exposure, and the term in parentheses is a transformed and normalised value of Human Development Index. The equation is only applicable to risk estimation at municipal level.

The calibrated risk model for the aforementioned parameters was considered to have a too low correlation for estimating risk at municipal level. Therefore, it is recommended as an alternative that the exposure maps be used as a proxy for risk.

The calibration of risk for earthquake-induced landslides was not possible due to the lack of consequences data for a meaningful statistical analysis (consequences data available for only 3 municipalities). This is due to the fact that the consequences for this category of landslides are often reported as caused directly by the earthquake shaking, and not by earthquake-induced landslides.



## **1 Introduction**

Landslides in El Salvador constitute an important natural hazard due to prevailing steep terrain covered with unconsolidated volcanic sediments and the frequent occurrence of extreme precipitation events and intense earthquakes. These high landslide hazard conditions occur in a country with the highest population density in the mainland Americas. Worldwide, among countries and territories with more than 5 million inhabitants, there are only 14 countries with a higher population density than El Salvador.

Two earthquakes in January and February 2001 caused more than 1000 casualties, 90% of whom were due to co-seismic landslides, most of them in one single event in a neighbourhood of the municipality of Santa Tecla. In November 2009, the tropical storm “Ida” delivered in only 5 hours more than 5 times the mean monthly precipitation in the San Vicente volcano, triggering numerous landslides that travelled more than 6 km from the source and killed almost 200 people.

The aforementioned facts combined with results from global risk evaluations, indicate that El Salvador is among the countries where drill-down studies are relevant for advancing the knowledge on landslide hazard and investigating the connections between the consequences on population and human development.

The present study performs a hazard evaluation for rainfall- and earthquake-induced landslides in El Salvador using a heuristic method and two statistically-based methods, namely the bivariate method and the weights-of-evidence method. Landslide inventories are used for calibrating hazard. Population exposure is calculated based on the resulting hazard maps and in the population density. Finally, risk correlations are attempted using databases of consequences (killed people).

## **2 Methods for hazard assessment**

The term “landslide” in this study refers to events involving gravity-driven rapid mass movement down-slope, like rockslides, debris flows, and rainfall- and earthquake-induced slides; which pose a threat to human life. Slow moving slides have significant economic consequences for constructions and infrastructure, but rarely cause any fatalities.

The present hazard assessment employed three different methods: the heuristic model used previously in the GAR 2009 and 2011 assessments, the bivariate method, and the weights of evidence method. These last two methods have a statistical basis that requires calibration from correlation with known incidents. Therefore, the methods were feasible and suitable for the present evaluation considering the availability of inventories. A single hazard map was obtained for

each triggering condition (rainfall and earthquake) from a weighted sum of the results of the three models.

The key modifications in the present model with respect to previous applications are:

- The increased resolution on the DEM and consequently the slope data. In previous studies 3 to 30 arc second resolutions were used, whereas the present study uses a 10 m resolution dataset.
- The earthquake triggering factor is based on a 500-year return period map of horizontal peak ground acceleration obtained from a probabilistic seismic hazard assessment (Marroquín and Benito, 2009).
- The rainfall triggering factor was estimated based on an extreme-value analysis of 1-day precipitation using data from 287 rain gauges during a 41-year operation period.
- The use of inventories for calibration of susceptibility and triggering factors, both for rainfall- and for earthquake-induced landslides.

## **2.1 NGI method**

To identify global landslide hazard and risk "hotspots", Nadim et al. (2006) adopted a simplified first-pass analysis method based on the procedure proposed by Mora and Vahrson (1994). The scale of their analysis was a grid of roughly 1km x 1km pixels where landslide hazard, defined as the annual probability of occurrence of a potentially destructive landslide event, was estimated by an appropriate combination of the triggering factors (mainly extreme precipitation and seismicity) and susceptibility factors (slope, lithology, and soil moisture). The principles of the method are depicted in Figure 1. The weights of different triggering and susceptibility factors were calibrated to the information available in landslide inventories and physical processes. The general approach used in the present study is a modified version of the approach used by Nadim et al. (2006).

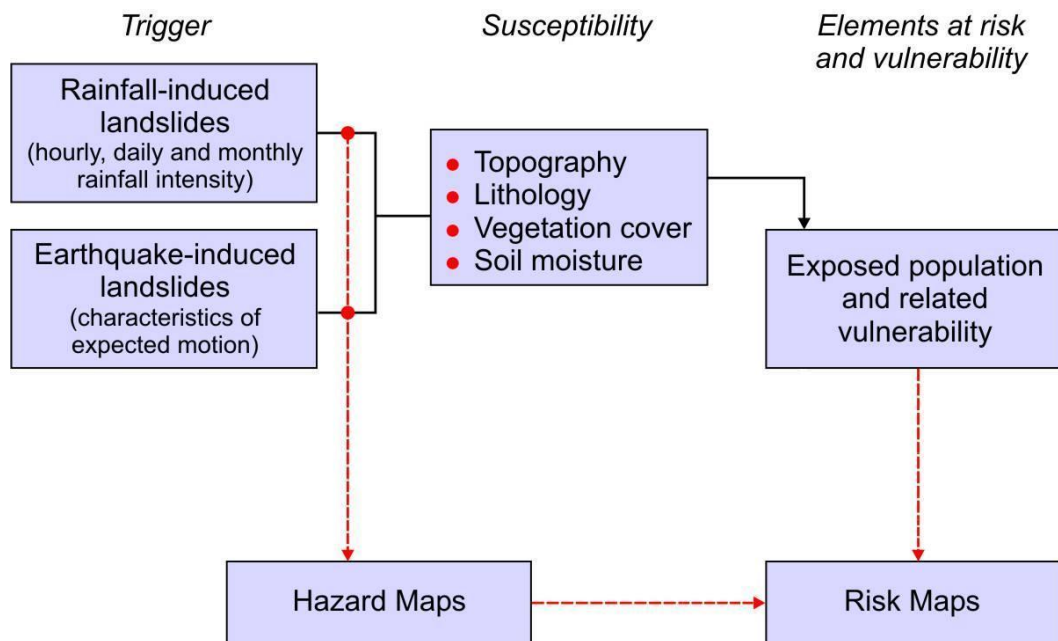


Figure 1. Schematic approach for landslide hazard and risk evaluation.

Primarily, the hazard is calculated as susceptibility multiplied by triggering factors. The hazard maps are divided in precipitation induced landslide hazard and earthquake induced landslide hazard. The landslide hazard indices are estimated using the following equations:

$$H_{NGIr} = (S_r \times S_l \times S_h \times S_v) \times T_p \quad (1)$$

$$H_{NGIe} = (S_r \times S_l \times S_h \times S_v) \times T_s \quad (2)$$

where  $H_{NGIr}$  and  $H_{NGIe}$  are landslide hazard indices for rainfall and earthquake induced landslides respectively,  $S_r$  is the slope factor within a selected grid,  $S_l$  is lithological (or geological) conditions factor,  $S_h$  describes the soil moisture condition,  $S_v$  is the vegetation cover,  $T_p$  is the precipitation factor and  $T_s$  describes the seismic conditions.

The values of the susceptibility and triggering factors are assigned using a heuristic approach that should account both for local experience and for a conceptually consistent physical basis (e.g.,  $S_l$  should increase when moving from one lithological unit to a relatively weaker one,  $T_s$  increases as earthquake peak ground acceleration becomes larger, etc.).

Finally, the maps with the landslide hazard indexes are classified in the desired number of descriptive hazard classes (e.g., negligible, low, medium and high). The boundaries between classes are defined such that the frequency of landslides per spatial unit within each class is equivalent to a conventionally defined frequency. The availability of a landslide inventory is useful at this stage for adjusting these class boundaries. The relative change of frequency between classes should be

consistent with the corresponding descriptions (i.e., landslide frequencies in the class “low” should be lower than in class “medium”, etc.).

## 2.2 Bivariate method

In cases when landslide inventories are available, it is desirable that the hazard assessment integrates the knowledge gained from the overlap of the observed incidents and the maps of the different susceptibility and triggering factors. The basis of the bivariate method is to estimate weights for the susceptibility and triggering factors using such overlaps. The combination of these weights results in hazard indexes that are reclassified into hazard classes. The details of the model as presented in this section are adapted from the description by van Westen (1997).

The steps of the bivariate method are listed below.

1. For a single susceptibility or triggering factor:
  - 1.1. Overlay the susceptibility or triggering factor map and the landslide inventory map. Herein, it is assumed that the values or categories of the factor map are represented in classes.
  - 1.2. Calculate landslide densities for each class of the factor map, as well as the overall landslide density in the entire map.
  - 1.3. Calculate a weight value for each class using a pre-established relation between the two densities calculated in the previous step.
  - 1.4. Reclassify the factor map using the weights calculated for each class.
2. Repeat step 1 for all susceptibility and triggering factors in order to convert all factor maps into weight maps.
3. Obtain hazard scores by combining the weight maps for all susceptibility and triggering factors using certain combination rules.
4. Reclassify the hazard scores into the desired number of classes such that the overlay with the landslide inventory is consistent in terms of frequency of occurrence per spatial unit.

The following formula is used for calculating the weights in step 1.3:

$$W_{ij} = \ln \left( \frac{Densclas_{ij}}{Densmap} \right) = \ln \left( \frac{\frac{N_{pix}(S_{ij})}{N_{pix}(N_{ij})}}{\sum_j \frac{N_{pix}(S_{ij})}{N_{pix}(N_{ij})}} \right) \quad (3)$$

where:

$W_{ij}$ : weight for class  $j$  within the susceptibility/triggering factor map  $i$ .

$Densclas_{ij}$ : density of landslides in class  $j$  within the susceptibility/triggering factor map  $i$ .

$Densmap$ : density of landslides in the entire map.

$N_{pix}(S_{ij})$ : number of pixels with landslides in class  $j$  within the susceptibility/triggering factor map  $i$ .

$N_{pix}(N_{ij})$ : number of pixels in class  $j$  within the susceptibility/triggering factor map  $i$ .

In this case, the combination rule used in step 3 is the sum of the weights pixel by pixel of all factor maps. Thus, for every pixel in the map:

$$W_{map} = \sum W_i \quad (4)$$

### 2.3 Weights of evidence method

The overlap between a landslide inventory and the maps of the susceptibility and triggering factors gives information not only on the positive evidence (i.e., overlap of observed incidents), but also on the negative evidence (i.e., overlap of areas with no incidents). The weights-of-evidence method estimates weights for the susceptibility and triggering factors using such overlaps (i.e., both positive and negative evidences). The combination of these weights results in hazard indexes that are reclassified into hazard classes. The details of the model as presented in this section are adapted from the description by van Westen (2002).

When each class of a factor map is crossed with the landslide inventory, there are four possible combinations of positive and negative evidences as indicated in Table 1.

Table 1. Possible combinations of presence and absence of class  $j$  in the  $i$ -th susceptibility or triggering map.

		Class $j$ in $i$ -th susceptibility or triggering factor map	
		Presence of class $j$	Absence of class $j$
Landslide inventory map	Presence of landslide	$N_{pix_1}$	$N_{pix_2}$
	Absence of landslide	$N_{pix_3}$	$N_{pix_4}$

where,

$$\begin{aligned}
 N_{pix_1} &= N_{pix}(S_{ij}) \\
 N_{pix_2} &= \sum_j N_{pix}(S_j) - N_{pix}(S_{ij}) \\
 N_{pix_3} &= N_{pix}(N_{ij}) - N_{pix}(S_{ij}) \\
 N_{pix_4} &= \sum_j N_{pix}(N_j) - \sum_j N_{pix}(S_j) - N_{pix}(N_{ij}) + N_{pix}(S_{ij})
 \end{aligned}$$

All terms on the right-hand side were defined in Eq. (3).

The steps of the weights-of-evidence method are the same as for the bivariate method (see section 2.2), except that the weight for each class (step 1.3 in section 2.2) is calculated following the procedure described below.

Weights to account for the effect of the presence or absence of a class in the occurrence of landslides are calculated as follows:

$$W_{ij}^+ = \ln \frac{\frac{Npix_i}{Npix_i + Npix_2}}{\frac{Npix_3}{Npix_3 + Npix_4}} \quad (5)$$

$$W_{ij}^- = \ln \frac{\frac{Npix_2}{Npix_i + Npix_2}}{\frac{Npix_4}{Npix_3 + Npix_4}} \quad (6)$$

where,

$W_{ij}^+$ : indicates the importance of the presence of class  $j$  (in the  $i$ -th factor map) for the occurrence of landslides.

$W_{ij}^-$ : indicates the importance of the absence of class  $j$  (in the  $i$ -th factor map) for the occurrence of landslides.

All terms on the right-hand side are defined in Table 1.

The presence of one class implies the absence of the other classes within the same factor map. Therefore, in order to obtain the weight for each class, the positive weight should be added to the sum of the negative weights of the other classes in the same factor map.

Then the weight  $W_{ij}$  for each class  $j$  in the  $i$ -th factor map is estimated as follows:

$$W_{ij} = W_{ij}^+ + \left( \sum_j W_{ij}^- \right) - W_{ij}^- \quad (7)$$

Finally Eq. (4) is used as the combination rule used for all the factor maps.

## 2.4 Combining results of hazard methods

A landslide hazard index  $H$  is obtained as a weighted sum of the results of the three methods described in sections 2.1, 2.2 and 2.3:

$$H = \sum w_k \overline{H}_k \quad (8)$$

where,

- $k$ : subscript index associated to each hazard method. In this particular case,  $k = 1, 2, 3$
- $w_k$ : priority weight assigned to the  $k$ -th method.  $w_k > 0$  and  $\sum w_k = 1$
- $\overline{H}_k$ : normalised hazard index for the  $k$ -th method. This normalisation is applied to the indexes of Eq. (1) and (2) and to the weights obtained from methods in sections 2.2 and 2.3 after applying Eq. (4).

The normalisation of the hazard index for each method is carried out such that the mean of the map for each method is zero. It is also a condition that the histograms should approximately follow the same type of distribution. Due to the procedure used to calculate the weights in the bivariate and the weight-of-evidence methods, they produce histograms that approximate normal distributions. The NGI method produces a histogram that approximates a log-normal distribution, so it should be transformed into a normal distribution first.

The evaluation of the hazard methods is performed separately for the two triggering conditions considered in this project: rainfall and earthquake. The resulting landslide hazard indexes obtained from Eq (8) are denoted as  $H_r$  and  $H_e$  for rainfall and earthquake triggering conditions, respectively.

Finally, the hazard indexes  $H_r$  and  $H_e$  are reclassified into the desired number of classes (e.g., negligible, low, medium and high) such that the overlay with the landslide inventory is consistent in terms of frequency of occurrence per spatial unit (i.e., higher frequency when increasing the hazard level).

### 3 Methods for evaluation of exposure and risk

The approach for evaluating exposure and risk is the same used in Nadim et al. (2006), in a European project on landslide risk (Jaedicke et al., 2010), in a World Bank project in South Asia (Vangelsten and Smebye, 2010), and in the GAR 2009 and 2011 assessments of landslide risk (Smebye and Kalsnes, 2009; Cepeda et al., 2010b). Physical exposure is evaluated as population exposure and risk as number of people killed, both normalized per spatial unit and per year.

#### 3.1 Evaluation of exposure

The physical exposure was calculated in terms of population exposure using the population density maps and the reclassified hazard maps. The percentage of population exposed to landslides by pixel is associated to the hazard level according to the values prescribed in Table 2.

Table 2. Percentage of total population exposed depending on hazard class.

Hazard class	Percentage of population exposed per pixel (%)
Negligible	0
Low	30
Medium	60
High	100

The resulting population exposure is denoted as  $PE$ , and subscripts are used to indicate the type of trigger associated to the hazard maps. Thus  $PE_r$  and  $PE_e$  denote population exposure to rainfall- and earthquake-induced landslides, respectively.

### 3.2 Evaluation of risk

Risk,  $R$ , is defined as annual frequency of people killed per spatial unit. The general form of the regression is:

$$\ln R = \beta + \alpha_0 \ln(PE) + \alpha_1 \ln\left(\frac{\overline{P_{1SN}}}{\overline{P_{1N}}}\right) + \dots + \alpha_i \ln\left(\frac{\overline{P_{iSN}}}{\overline{P_{iN}}}\right) + \dots + \alpha_n \ln\left(\frac{\overline{P_{nSN}}}{\overline{P_{nN}}}\right) \quad (9)$$

where,

$\beta, \alpha_0, \alpha_1, \dots, \alpha_i, \dots, \alpha_n$ :	intercept and regression coefficients
$PE$ :	population exposure
$n$ :	number of socio-economic parameters
$P_i$ :	$i$ -th socio-economic parameter
$\overline{P_{iSN}}$ :	sub-national level value for the $i$ -th socio-economic parameter
$\overline{P_{iN}}$ :	national level value for the $i$ -th socio-economic parameter

Socio-economic parameters that have been used in previous risk evaluations performed by NGI include:

- Percent forest cover
- Percent arable land
- Percentage population without access to clean water
- Percentage population without access to health facilities
- Human Development Index (HDI)
- Gender Development Index (GDI)
- Human Poverty Index (HPI)

The sub-national level is defined by the level of administrative division used to report the socio-economic parameters and the consequences. Since landslide hazard and risk can have abrupt spatial variations, in most cases mainly controlled by topography and lithology, it is preferred that the level of administrative division used in the analysis corresponds to the smallest possible spatial units. Therefore, district level is preferred to province level, municipal level to county (or department) level, etc.

The values of mortality risk,  $R$ , for calibration are obtained from inventories of consequences, expressed as number of people killed. In the evaluations performed by NGI, the source for casualties has been the DesInventar database (<http://www.desinventar.net/>).

The calibration of Eq. (9) is performed at the same administrative level as the available input data, defined by the coarsest administrative level in the socio-economic parameters and consequences. Therefore, Eq. (9) should be used for estimating risk only at the same administrative level that was used for calibration.

## 4 Datasets

A wide range of data was used to assess the risk and hazard analysis. The focus lay on raster based formats as they possess information on the chosen resolution. For this study, the available resolution was 10-m cells.

Primarily, the data was based on a digital terrain model originally obtained from interpolation of topographic contours. From this terrain model, the following terrain parameters were estimated: slope, planar and profile curvature, aspect, and stream networks.

Other factor maps, such as lithology or landcover, were based on shapefiles. The rainfall data was provided as a raster (average monthly and annual precipitation).

The road network was derived by merging four classification levels (first to fourth order roads, including for example the Pan-American Highway).

Inventories were available for both, single major triggering events (i.e., event-based inventories), and as a collection of incidents over an observation period.

The main datasets used for the evaluations are listed in Table 3.

Table 3. Main spatial datasets used for the evaluations.

Data	Format	Source	Secondary Products
DEM	Raster	DGOA	Slope, Elevation, Curvature, Aspect, Hillshade, Hydrology (Stream order and network, Basins, etc.)
Land use	Vector and Raster	DGOA	
Lithology	Vector and Raster	DGOA	
Rainfall	Raster	DGOA	Rainfall parameter calculated by accumulating 5-month precipitation over the wettest period
Roadnetwork	Vector	DGOA	Merged
PGA	Raster	Marroquín and Benito (2009)	
Population	Raster	Landscan Worldwide Population data	
HDI	Vector	UNDP	
Inventories	Vector	DGOA, USGS, DesInventar	

Notes:

DGOA: Dirección General del Observatorio Ambiental, Ministry of Environment and Natural Resources of El Salvador.

USGS: United States Geological Survey.



Most of the available data was given in a rather national projection system – NAD 1927 Lambert Conformal Conic.

Various other data, such as Landscan Population and in general “external” data (i.e., data not from DGOA), were in GCS 1984 or ELS Lambert Conformal Conic.

Most of the given information needed to be prepared to process further. This implied smaller modifications like conversions into raster or more complex ones like computing new rasters using models.

All datasets for susceptibility and triggering factors had to be reclassified in order to enable the application of the hazard methods.

## 4.1 Topography

Difficulties appeared by using the given DEM as a source for many other parameters (slope, aspect, curvature etc.) are derived on the basis of the DEM. Several spurious areas occur across the country (see Figures 2 and 3). This is due to limitations in the processing capacity during the calculation of the DEM, which required splitting the country in eight zones. These zones were merged into a national DEM and spurious topographical features were generated during the merging process. These spurious features consist in abrupt changes in topography. In order to smooth these spurious zones, an interpolation with a moving window was carried out.

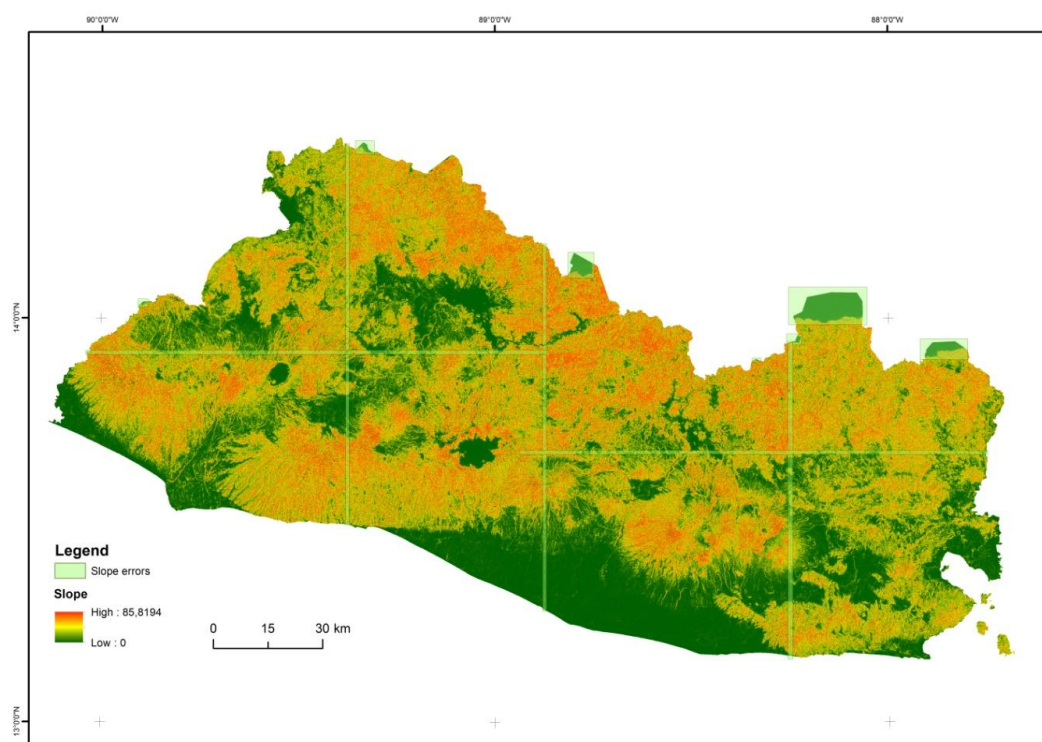


Figure 2. Slope map of El Salvador showing strips and areas with spurious slope values.

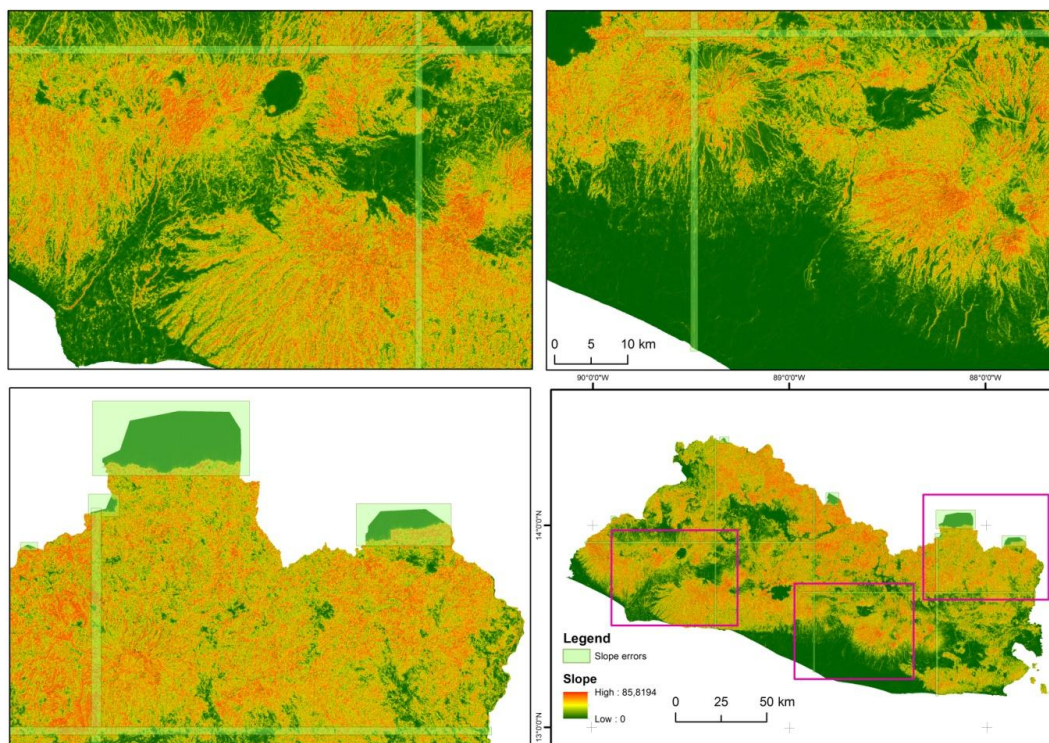


Figure 3. Details of areas with spurious data in the digital terrain model.

Moreover, some border areas with Honduras are not defined as they have been included in zones of territorial disputes. Some given spatial information do not show data in these areas while others have detailed data provided. As mentioned before the DEM was originally derived from the interpolation of contour lines, which were not available in these border zones (see lower left panel in Figure 3).

Several possibilities to define the data and remove the inaccuracies were taken into consideration, such as using SRTM data with a resolution of 30 m. This data could replace the spurious areas and give additional information. However, removing these areas as a last step of the calculations is the simplest and least time consuming method. Moreover, implementing SRTM data, which would also imply to resample and causing loss of information and, as mentioned before, some parameters do not have information in those areas.

The slope factor was reclassified in five classes referring to familiar class breaks. Previous experiences of similar NGI projects was the basis for the following classification. Landslides are most likely in the slope degree range from 18 to 40 degrees, which form the two highest classes. Slopes with an angle of more than 40 degrees are less prone to landslides due to the predominance of more competent lithologies, therefore, the slope factor is decreasing again.

Table 4. Classification of slope angle.  $S_r$  is the slope susceptibility factor used in the NGI method.

Range of slopes angle (unit 1/100 degrees)	Classification	$S_r$
0000 – 0100	Very low	0
0101 – 0600	Low	1
0601 – 1200	Moderate	2
1201 – 1800	Medium	3
1801 – 2400	High	4
2401 - 4000	Very high	5
>4001	Medium	3

*Note:* For slopes which angle is less than  $1^\circ$  (i.e. for flat or nearly flat areas),  $S_r$  is set equal to zero because the resulting landslide hazard should be zero even if other factors are associated to higher susceptibility.

The reclassified slope map is shown in Figure 4.

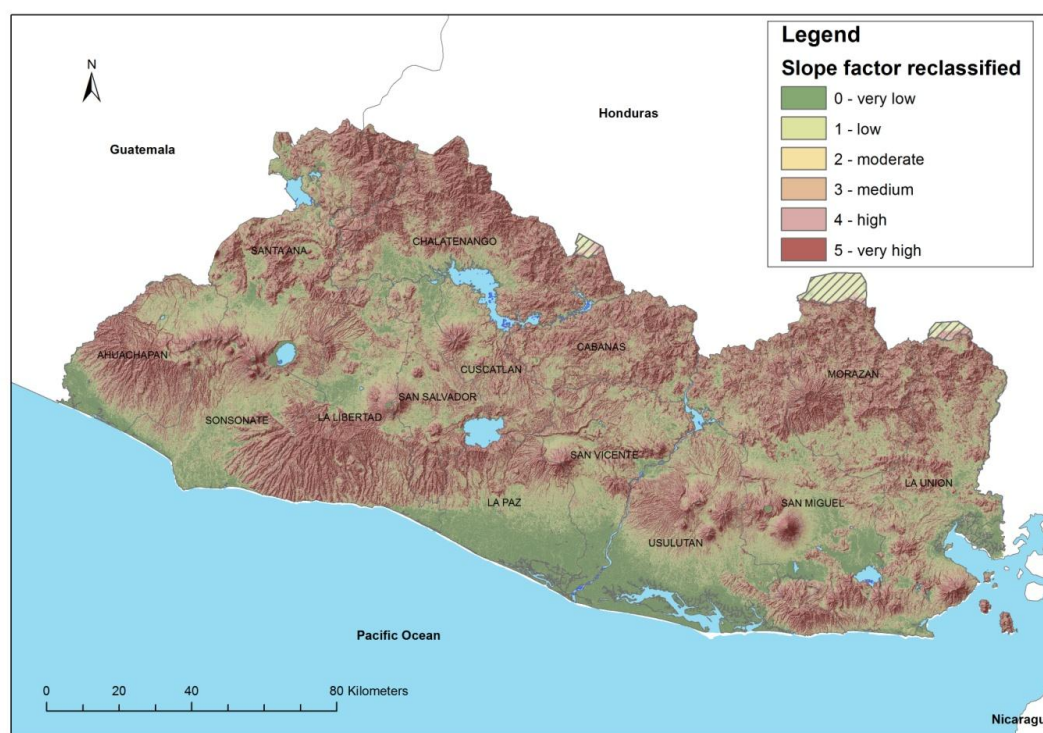


Figure 4. Reclassified slope map.

For the weights of evidence and bivariate methods additional terrain parameters were derived from the DEM, namely aspect, planar and profile curvature, and stream order. In the stream network the maximum value of stream order is seven, which means, the smallest ramification and a main river branch is one.

## 4.2 Lithology

This is probably the most difficult parameter to assess. Ideally, detailed geotechnical information should be used but, at the national scale, only a general geological description is available. Rock strength and fracturing are the most important factors to evaluate lithological characteristics, and these characteristics can vary greatly over short distances.

In general, the geology features mainly volcanic rocks and minor metamorphic rocks. The volcanic rocks can be subdivided by their age into tertiary and quaternary. The latter is responsible for shallow failures on slopes along the young volcanic chain, whereas deep seated landslides are more likely along the northern mountain range which mainly consists of tertiary rocks (personal communication, Manuel Díaz, 9/8/2012). Garcia-Rodriguez et al. (2008) also provided a classification into four classes (hard rock, soft rock, consolidated and unconsolidated soil).

In order to obtain a comprehensive classification, both the expert base approach of DGOA and a validation with the given landslide inventory was carried out. The original classification provided by DGOA and used in Garcia-Rodriguez et al. (2008) was adjusted by comparing with the available landslide inventories. A simplified classification in five classes is shown in table 5. The actual total number of lithological units is 27. Within each lithological formation there are units with varying susceptibility levels, therefore some formations are associated to more than one susceptibility factor.

Table 5. Summarized reclassification of lithology in terms of lithological formations.

Formation	$S_l$
Water bodies	0
Bálsamo	1, 3
Cuscatlán	1, 4
Morazán - Chalatenango	1
San Salvador	1, 4, 5
Grupo Yojoa	1
Todos santos	2
Valle de ángeles	2
Chalatenango	3, 4, 5
Morazán	3, 5

Since the present study does not account for hazard and risk assessment due to submarine landslides, all water bodies are set to a susceptibility factor equal to zero.

A total of 5 susceptibility classes were used in the analyses, as shown in Table 5. Usually old rocks are stronger than young rocks. Plutonic rocks will usually be

strong and represent low susceptibility. Strength of metamorphic rocks is variable, but these rocks often have planar structures such as foliation and therefore may represent higher susceptibility than plutonic rocks. Lava rocks will usually be strong, but may sometimes be associated with tuff (weaker material). Therefore, areas with recent volcanism are classified as high susceptibility. Sedimentary rocks are often very weak, especially young ones.

Figures 5 and 6 show the lithological formations and the reclassified lithology according to Table 5.

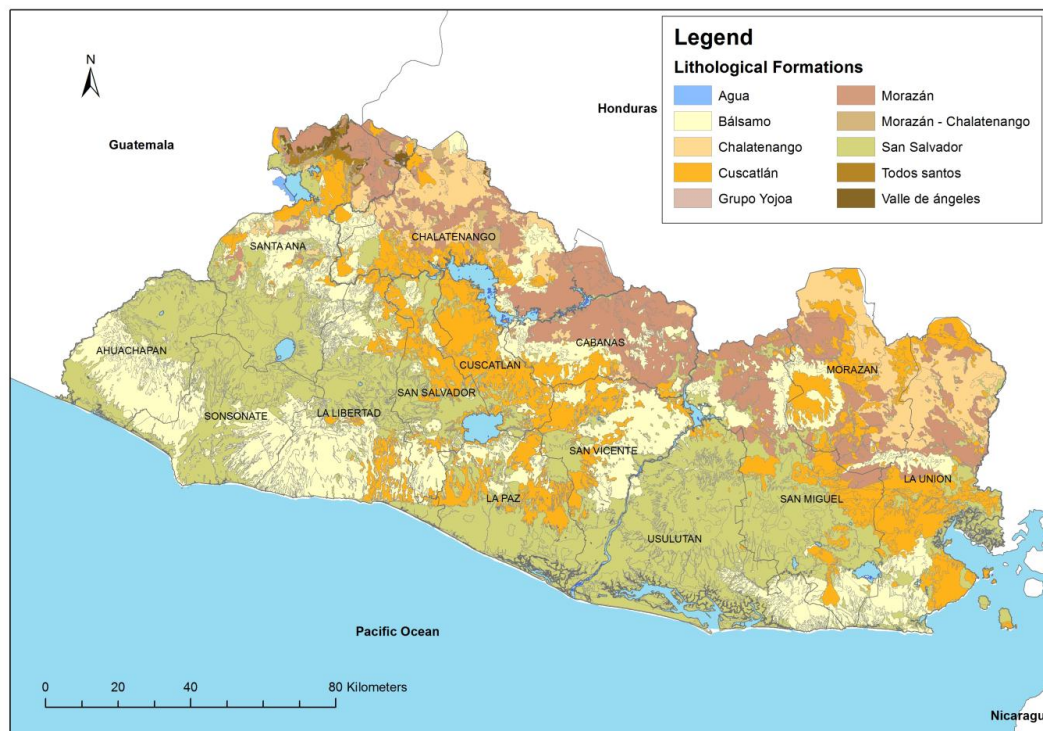


Figure 5. Lithological formations.

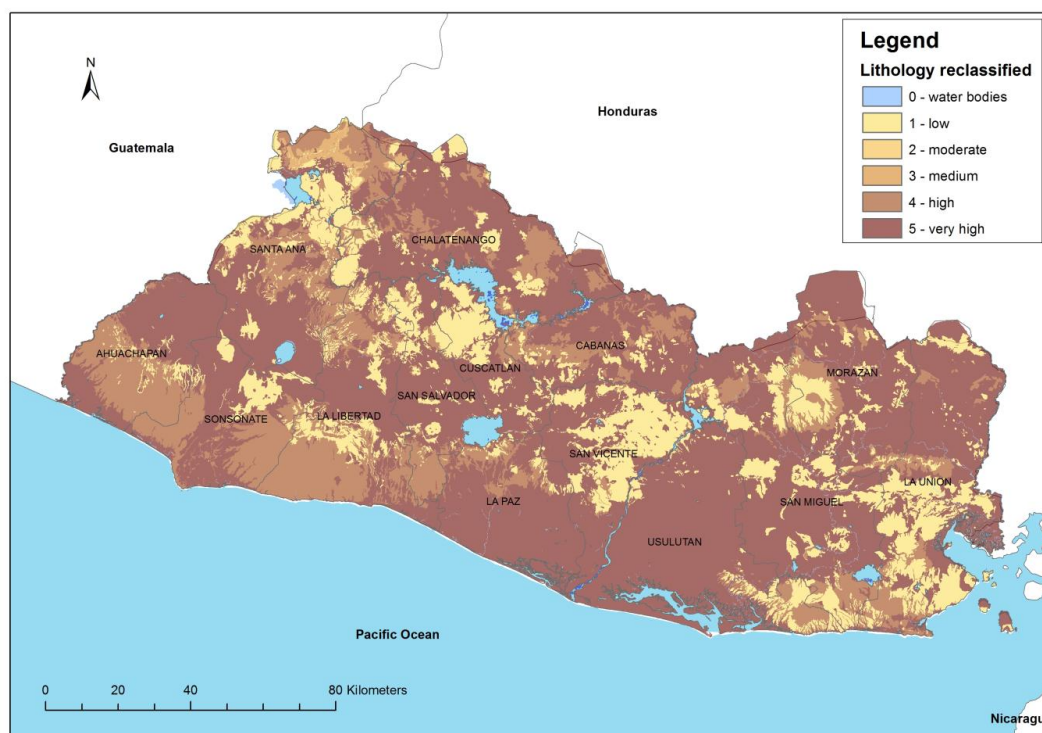


Figure 6. Reclassified lithology.

### 4.3 *Moisture*

Soil moisture data was downloaded from IRI/LDEO and was based on data derived from NOAA (<http://iridl.ldeo.columbia.edu/SOURCES/.NOAA/.NCEP/.CPC/.GMSM/.w/>). The pixel size is 55 km, which is too coarse for the size of the study area (roughly 200 km x 100 km). The country area was split into pixels (15 for the whole country) corresponding to the global moisture data in order to explore a correlation between rainfall and relevant soil moisture. As the correlation was very poor, it was discarded to perform an indirect estimation of soil moisture based on precipitation.

An assessment of rainfall-thresholds in the San Salvador volcano, estimated that the critical antecedent precipitation for landslide triggering is 150 days (Cepeda, 2009). This antecedent precipitation can be considered as a proxy for soil moisture before the onset of a triggering event. Based on the above, cumulative precipitation was calculated over the wettest 5-month period (from June to October). The cumulative 5-month precipitation was reclassified in three classes in agreement with previous hazard evaluations. The resulting map is shown in Figure 7.

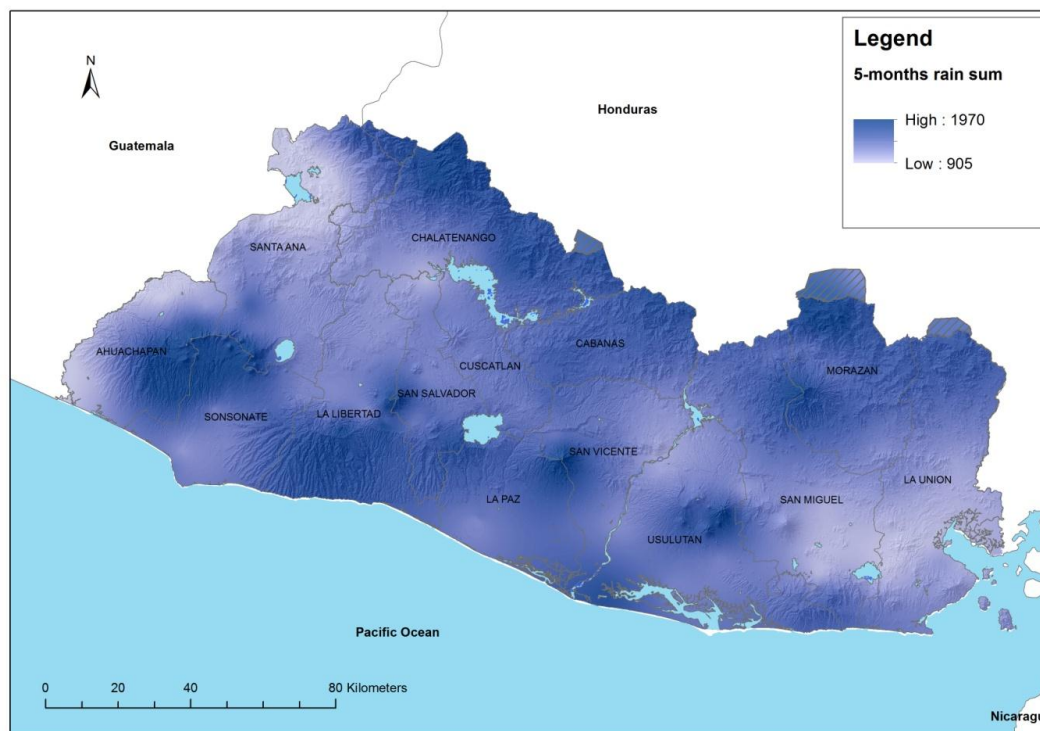


Figure 7. Cumulative precipitation over the 5-month wettest period (June-October).

#### 4.4 Land cover

The land cover database (actually “land use” when translated directly from the Spanish name) has a wide range of different classes and subclasses of vegetation cover, which have been translated into five categories with respect to non-resistance to landslides. See Table 6.

Table 6. Reclassification of land cover.

Description	Group	Category of vegetation cover w.r.t. non-resistance to landslides.
Continuous urban area	Urban areas	5
Discontinuous urban area	Urban areas	3
Precarious urban area	Urban areas	5
Progressive urban area	Urban areas	2
Commercial or Industrial zone	Industrial zones	1
Harbour zone	Industrial zones	1
Airport	Industrial zones	1
Touristic and archeological areas	Industrial zones	3
Mining areas	Mining	5
Mine waste areas	Mining	5

Construction zones	Mining	4
Urban green zones	Artificial green zones	2
Sport and recreation areas	Artificial green zones	1
Staple grains	Annual crops	4
Vegetables	Annual crops	2
Cultivated pasture	Pasture	5
Natural pasture	Pasture	5
Annual crops	Mixed crops	5
Mix of crops and pasture	Mixed crops	4
Mix of crops, pasture and vegetation	Mixed crops	4
Agro forestry systems	Mixed crops	2
Conifer forest	Forests	4
Blended forest	Forests	4
Mangrove forest	Mangrove	1
Monospecific forest plantations	Forests	3
Gallery forest	Forests	3
Natural herbaceous vegetation	Shrub vegetation	3
Low shrub vegetation	Shrub vegetation	5
Sclerophyllous or spiny vegetation	Shrub vegetation	1
Paddocks	Shrub vegetation	2
Beach bush vegetation	Shrub vegetation	1
Ecotonal zones	Shrub vegetation	2
Beaches, dunes and shoals	Shrub vegetation	1
Lavas	Shrub vegetation	5
Areas with scarce vegetation	Shrub vegetation	5
Burned zones	Shrub vegetation	5
Interior marshes	Wetlands	1
Marshy prairies	Wetlands	1
Aquatic vegetation over water bodies	Wetlands	1
Marine swamps	Wetlands	1
Salterns	Wetlands	1
Aquaculture perimeter	Wetlands	1
Rivers	Water bodies	0
Lakes and lagoons	Water bodies	0
Coastal lagoons and estuaries	Water bodies	0
Estuaries	Water bodies	0
Sea and ocean	Sea and ocean	0
Nurseries with ornamental plants and others	Industrial zones	1
Other irrigated crops	Annual crops	3
Banana plantations	Permanent crops	3

Coffee	Permanent crops	5
Oil palm trees	Permanent crops	3
Fruit-trees	Permanent crops	3
Sugar cane	Permanent crops	5
Pineapple crops	Permanent crops	2
Deciduous forest	Forests	2
Evergreen forest	Forests	2
Semi deciduous mixed forests	Forests	2

The distribution of groups of land cover is presented in Figure 8.

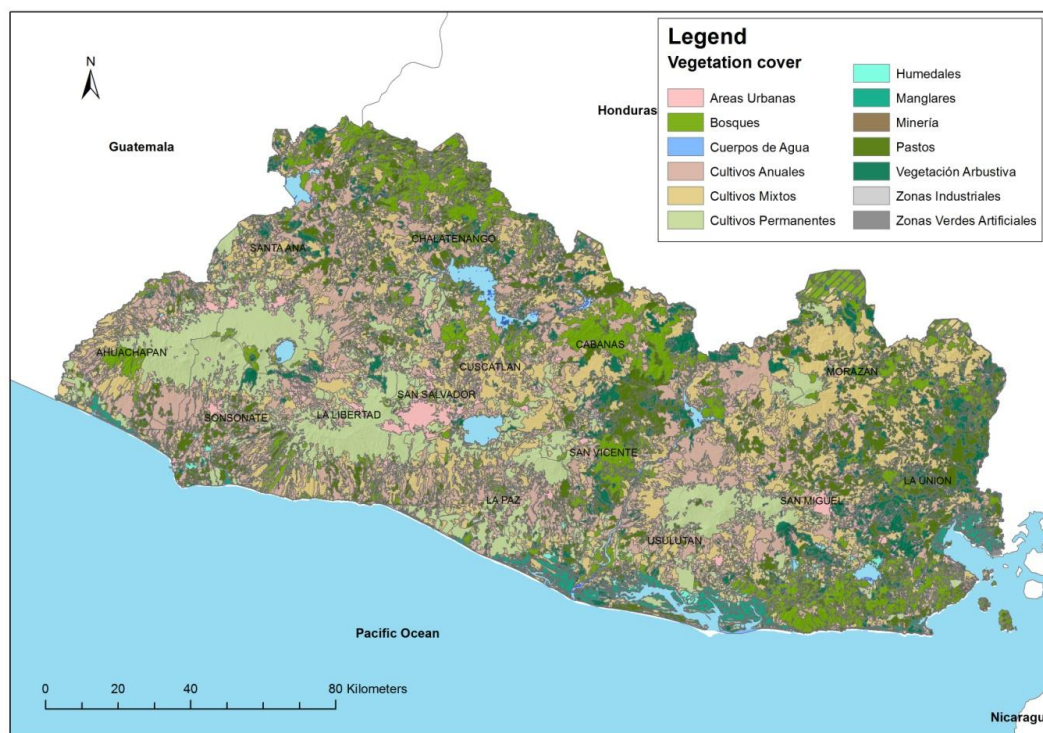


Figure 8. Land cover.

The classification of the resistance of the land cover units in Table 6 was done by combining the expert input from colleagues at the DGOA with interpretation from overlaying the land cover map with the landslide inventory. The land cover non-resistance was associated with two different sets of susceptibility factors for rainfall and earthquake induced landslides, based on interpretations from previous hazard assessments (e.g., Smebye and Kalsnes, 2009). Table 7 shows the corresponding susceptibility factors for  $S_v$  associated to these five categories.

Table 7. Vegetation cover index  $S_v$  associated to categories of vegetation cover with respect to non-resistance to landslides.

Category of vegetation cover w.r.t. non-resistance to landslides	Vegetation cover index $S_v$ for rainfall-induced slides	Vegetation cover index $S_v$ for earthquake-induced slides
1	0.8	0.9
2	0.9	0.95
3	1.0	1.0
4	1.1	1.05
5	1.2	1.1

Note: all water bodies were assigned  $S_v = 0$ .

Figures 9 and 10 show the distribution of vegetation cover index for rainfall- and earthquake-induced landslides, respectively.

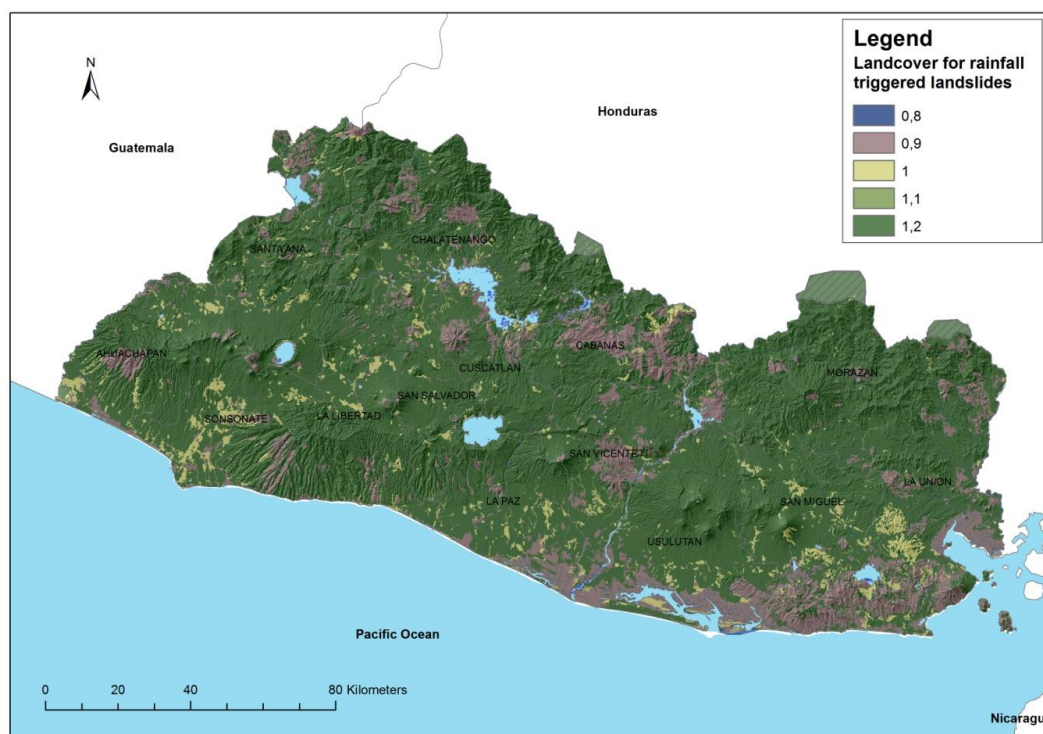


Figure 9. Landcover reclassified for rainfall trigger.

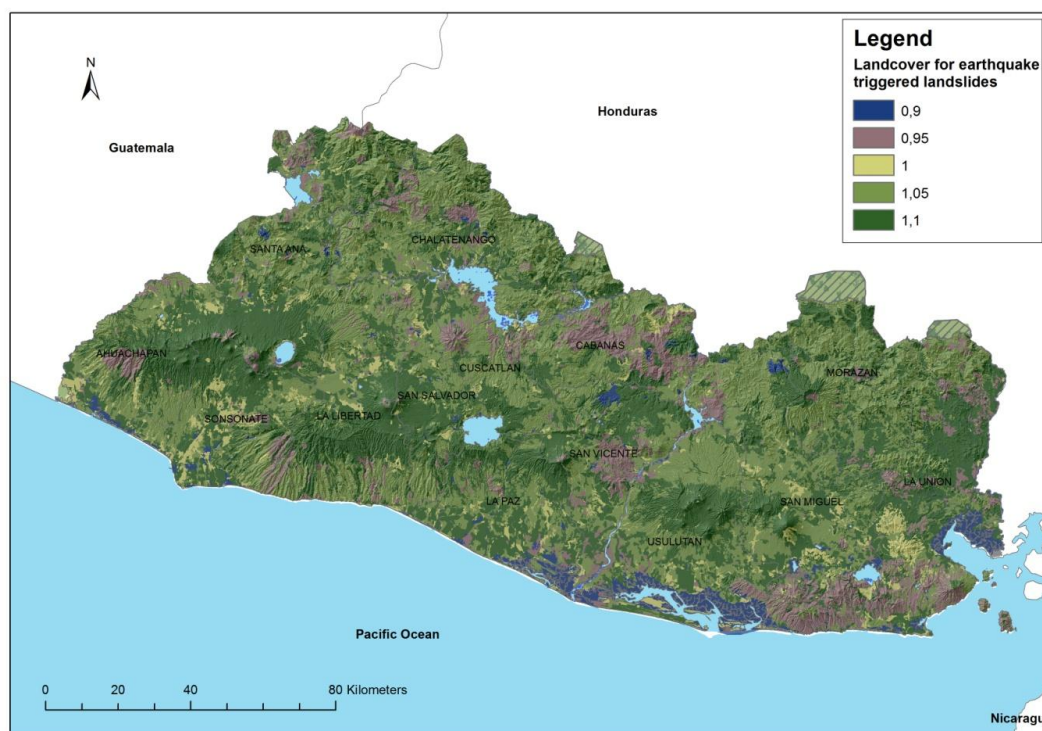


Figure 10. Landcover reclassified for earthquake trigger.

#### 4.5 Road network

When roads run across steep terrain, the presence of cut slopes and embankment fills may constitute an important factor for locally increasing the susceptibility to landslides. This has been evidenced in previous assessments (e.g., Cepeda et al., 2010b). Additionally, several incidents in the inventories from El Salvador have occurred on cut/fill slopes along roads. In order to account for the above in the hazard assessment, the road network was included as a susceptibility factor in the bivariate and weights-of-evidence methods. Since the road network theme is a vector of type line, and the areas of cut/fill slopes extend some distance to the sides of the road centre line, it was necessary to create buffers. These were defined using distances set to 50, 100, 150 and 200 m.

#### 4.6 Rainfall trigger

The precipitation triggering factor was evaluated based on an extreme-value analysis of 287 rain gauges over an operation period of 41 years. The distribution of the rain-gauge network is shown in Figure 11. In order to illustrate the high spatial resolution of the network (and of the rainfall data) with respect to real-time global precipitation data, the rain gauges are overlain in Figure 11 with the tiles of rainfall data estimated from satellite observations by NASA's TRMM mission (<http://trmm.gsfc.nasa.gov/>). The TRMM data produces one single estimate of precipitation in real-time per each tile.

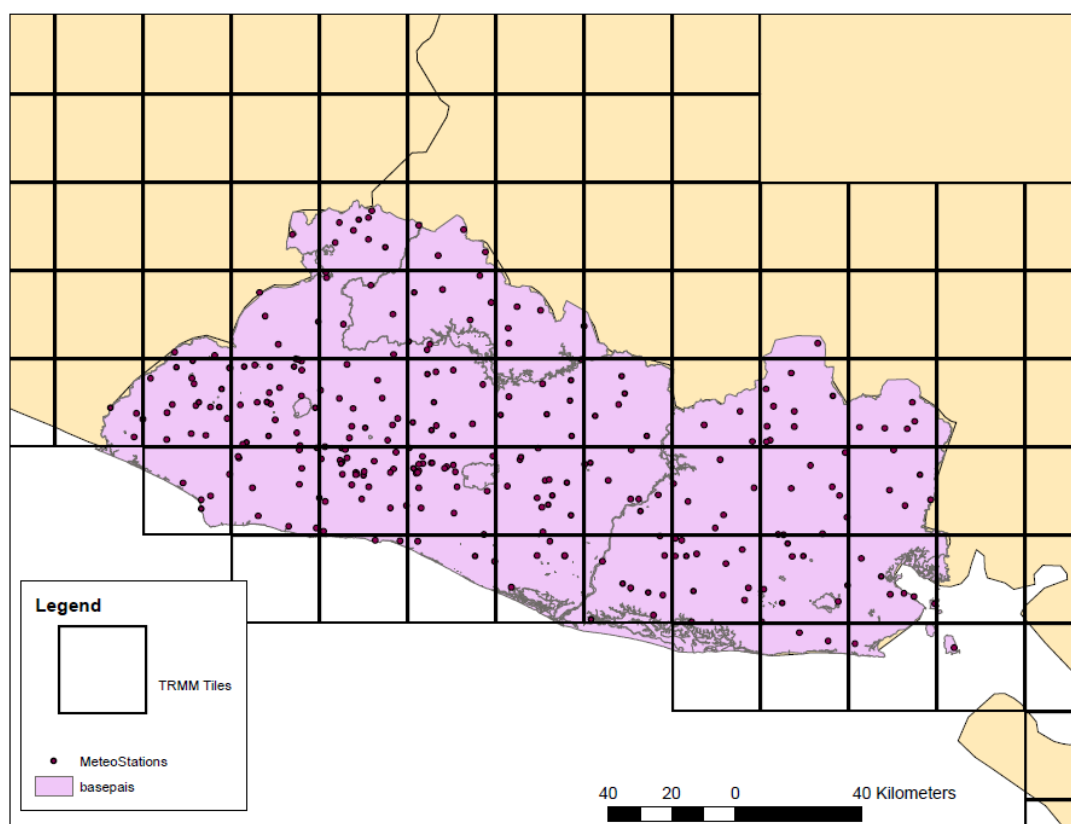


Figure 11. Distribution of rain gauge stations and tiles of TRMM data. Courtesy of NASA's Dalia Kirschbaum.

Since only few rain gauges provide data for the complete 41-year period of observation, and in order to have a sufficient spatial distribution of extreme values, the estimates of the maximum daily precipitation were evaluated for a 10-year return period. The extreme values were spatially interpolated and a smoothing filter was applied to the interpolated raster. The raster values were linearly mapped to the minimum and maximum triggering factors  $T_r$  (1 and 3). The resulting spatial distribution of precipitation triggering factors is presented in Figure 12.

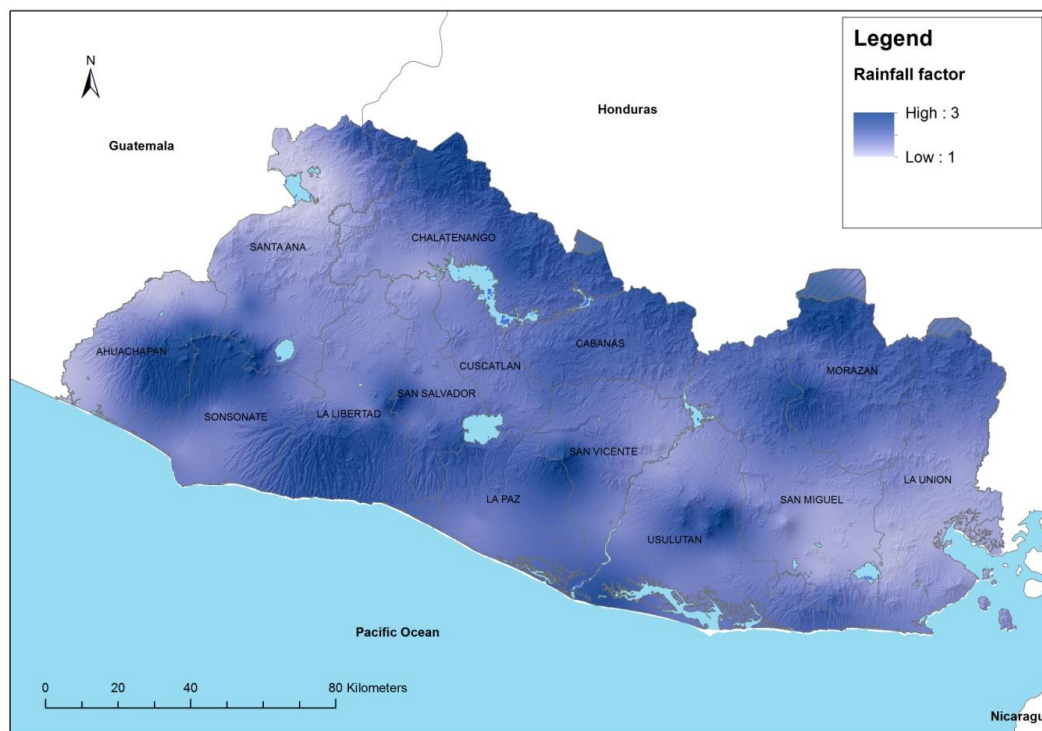


Figure 12. Rainfall triggering factor.

#### 4.7 Earthquake trigger

The dataset used for characterising the seismic triggering factor was the expected horizontal Peak Ground Acceleration (PGA) with a 500-year return period calculated by Marroquín and Benito (2009) in a probabilistic seismic hazard assessment, and provided for this study by DGOA in the form of a raster map.

The polygon inventory of earthquake-induced landslides available for calibrating hazard in the present study is an event-based inventory prepared as part of a project financed by the Japanese International Cooperation Agency (JICA). This inventory contains landslides triggered by two earthquakes in 2001: a 7.7  $M_w$  subduction earthquake that occurred on 13 January and a 6.4  $M_w$  upper-crustal earthquake on 13 February. In order to calibrate the susceptibility and triggering factors in the bivariate and the weights-of-evidence methods, it is desirable to use the values of PGA corresponding to the ground motions induced during these two earthquakes. For this purpose, simulations of ground motions were carried out using the source mechanisms presented by Benito et al. (2004) and Cepeda et al. (2004), and the ground motion attenuation equations presented by Cepeda et al. (2004), which were derived from a regression of recorded earthquake motions during the two earthquakes. The seismic sources and the results of the simulated PGA for each earthquake are presented in Figures 13 and 14

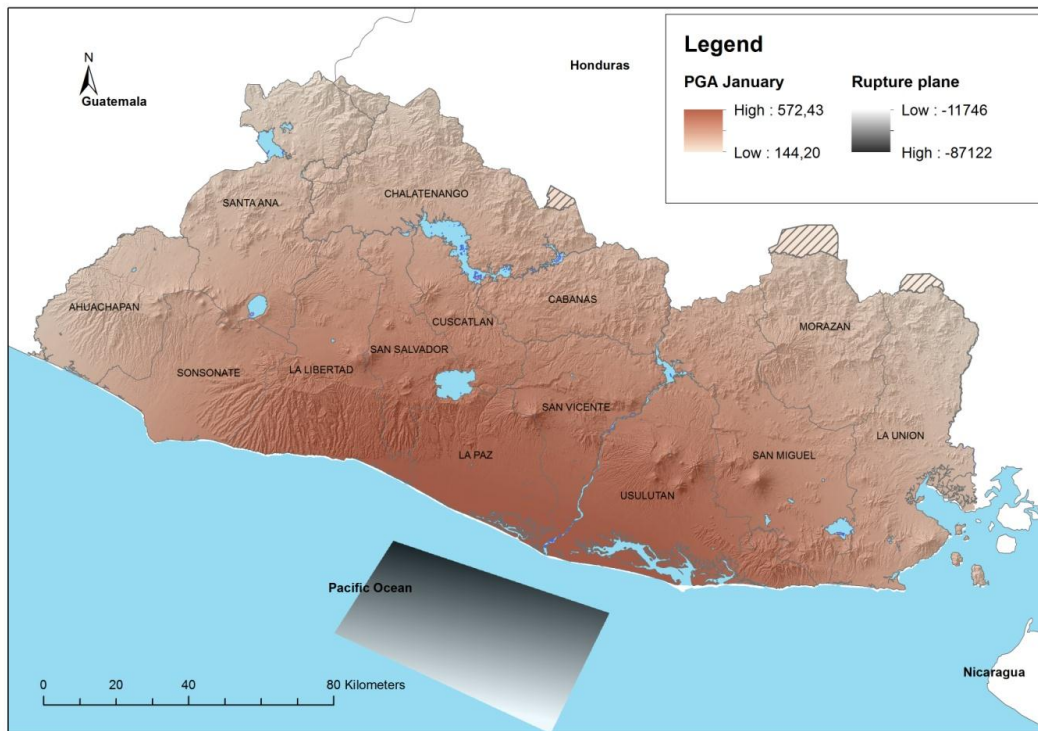


Figure 13. Simulated peak ground accelerations in  $\text{cm/s}^2$  due to the 13 January 2001 earthquake using attenuation equations from Cepeda et al. (2004) and seismic source parameters and geometry from Belen et al. (2004) and Cepeda et al. (2004).

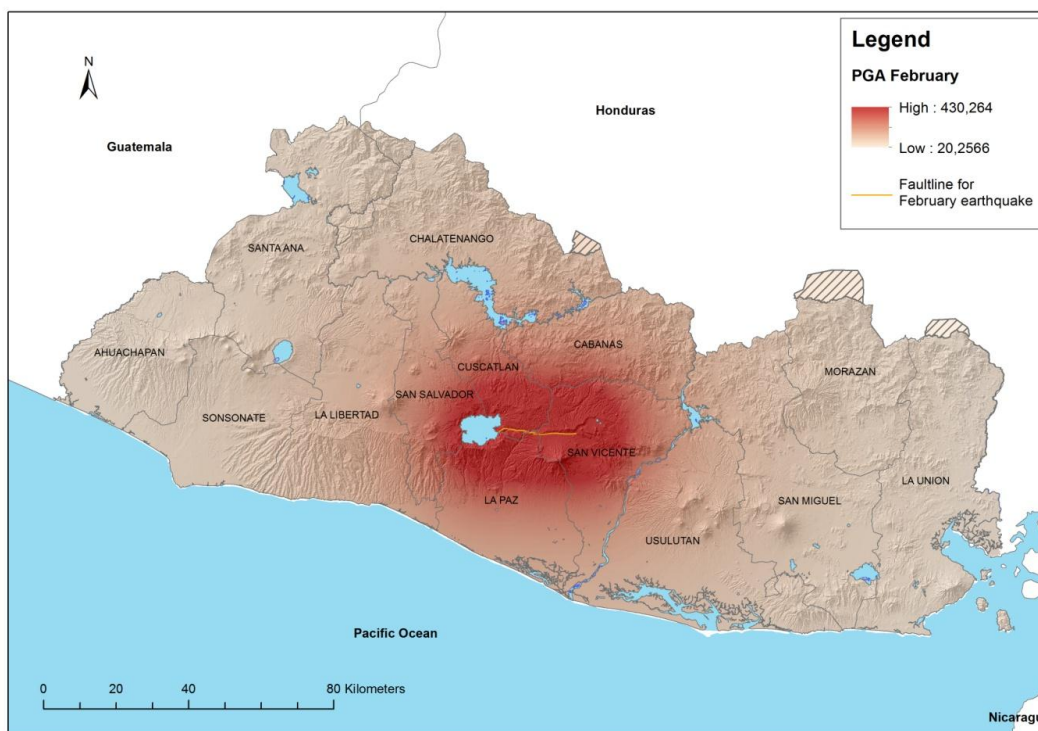


Figure 14. Simulated peak ground accelerations in  $\text{cm/s}^2$  due to the 13 February 2001 earthquake using attenuation equations and rupture plane suggested by Cepeda et al. (2004).

The PGA map for calibration with the landslide inventory is a mosaic of the maps shown in Figures 13 and 14, where each pixel is assigned the maximum PGA from the two maps.

The map of PGA from the probabilistic seismic hazard assessment by Marroquín and Benito (2009) is used for the actual evaluation of hazard. The map is presented in Figure 15. This raster is reclassified into the earthquake triggering factor  $T_s$  by linearly mapping to the maximum and minimum values of the factor (0.01 and 10).

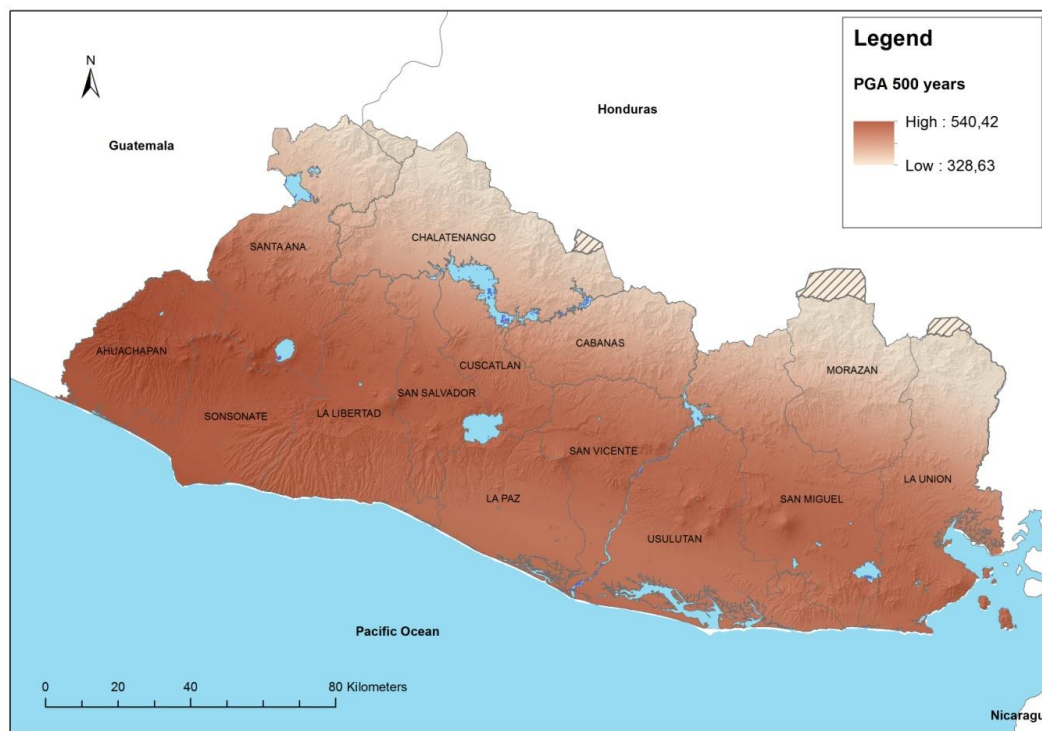


Figure 15. Horizontal peak ground acceleration in  $\text{cm/s}^2$  for a 500-year return period based on the probabilistic seismic hazard assessment in Marroquín and Benito (2009).

#### 4.8 Population density

The population data was extracted from the worldwide available dataset. The pixel cell size is 900 m, which is good enough to detect major cities and rural areas. As population data on municipality level was also available, a test was conducted to derive and decide for the most accurate data. The available shapefile information was based on the census of 2007, whereas the Landscan population data showed a good agreement with the total population of the latest projections. Considering the above, and that it is preferable to have pixel-based distribution of population for exposure purposes (rather than per administrative division), the Landscan data was used for estimating physical exposure of population. The map of population density is presented in Figure 16.

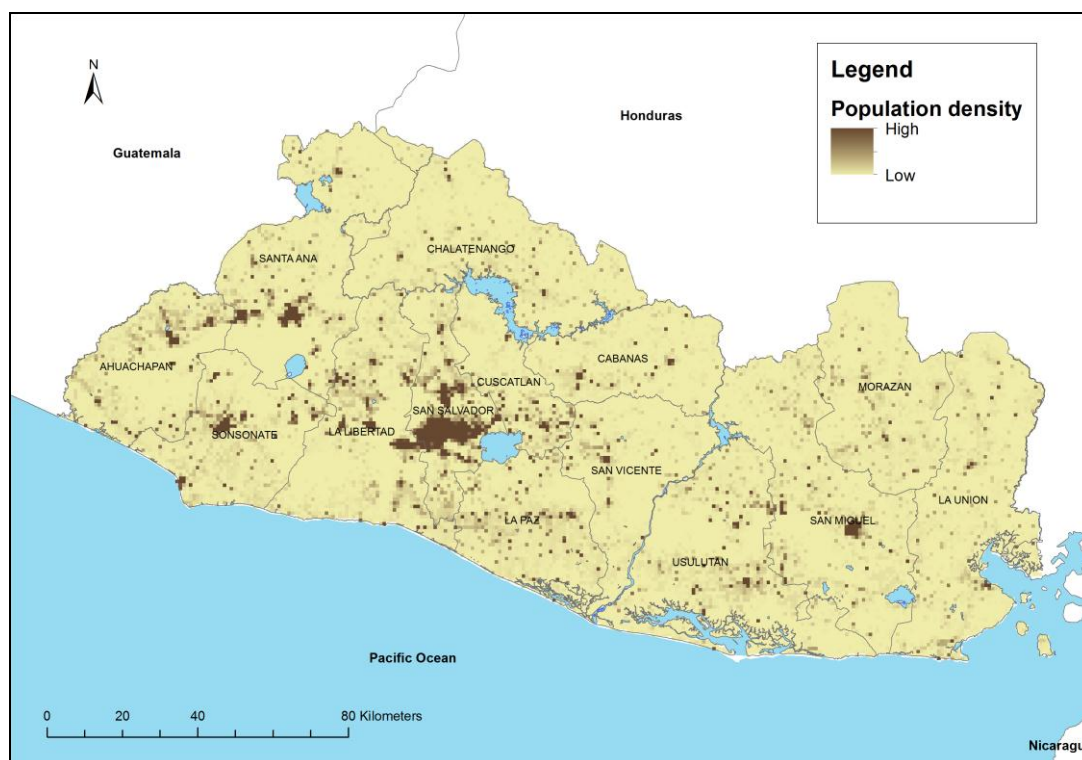


Figure 16. Map of population density.

#### 4.9 Socio-economic parameters

Socio-economic parameters were available from (UNDP and FUNDAUNGO, 2009) at municipal level, which is the most detailed resolution in the consequences data from DesInventar. All the available socio-economic parameters were strongly correlated with Human Development Index, HDI, so it was decided to use HDI as the sole parameter. Other parameters that are conceptually not strongly correlated with HDI were available only at national or departmental level (e.g., the parameters listed section 3.2). Figure 17 shows the spatial distribution of HDI. When comparing with the population density shown in Figure 16, it is evident that the highest HDI municipalities are located in the main urban centres in the metropolitan area of San Salvador (at the centre of the country), in Santa Ana and San Miguel.

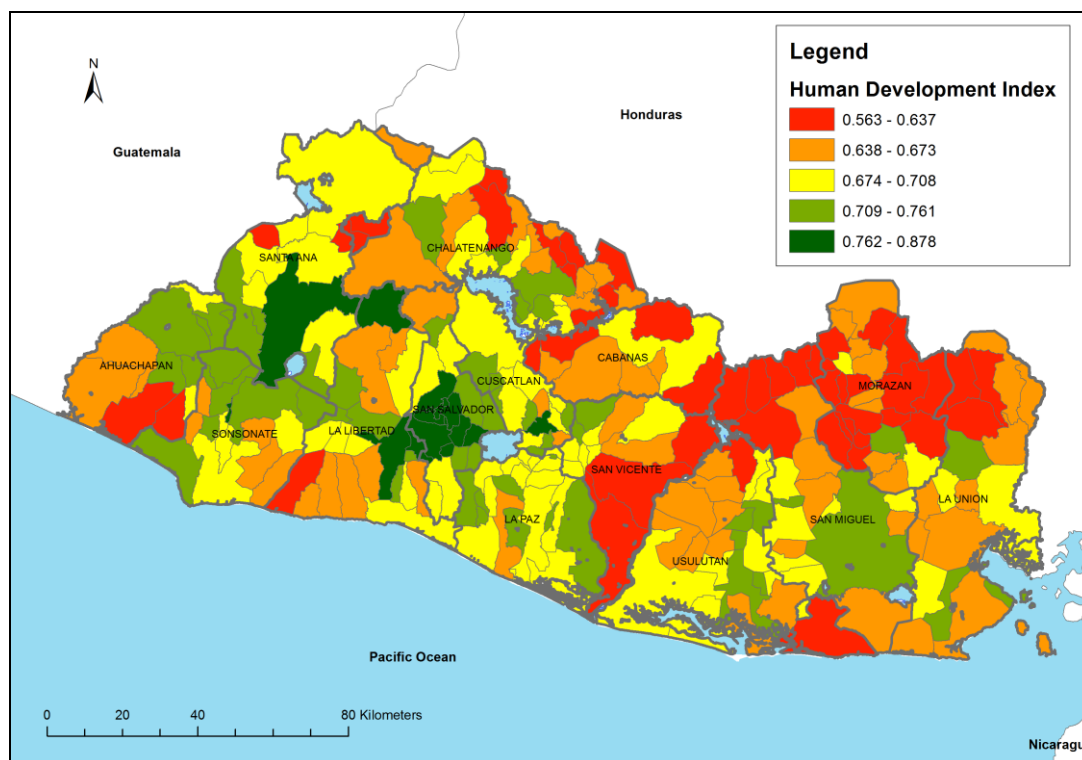


Figure 17. Human development index per municipality.

#### 4.10 Inventories

For the present study, the following inventories were available:

- Event-based inventories. These were prepared by mapping events using remote-sensing techniques. The events are mapped as polygons. Consequences data are not provided for every incident.
  - Rainfall-induced landslides associated to Hurricane Mitch in 1998. Crone et al. (2001). Project financed by the United States Agency for International Development, USAID. Data downloaded from <http://www.usgs.gov>
  - Earthquake-induced landslides associated to the 13 January and 13 February earthquakes in 2001 (see section 4.7 for details). Kakiuchi (?). Project financed by the Japanese International Cooperation Agency, JICA. Data provided by DGOA.
- Historic inventory. A historic inventory was provided by DGOA for the present study. All events in this inventory were reported due to the consequences in roads or in inhabited areas, but the consequences are not systematically reported because the focus is on the characterization of the landslide features from a geological perspective. The triggering factors are identified as rainfall, earthquake, volcanic eruption or other causes. The period of the inventory is from 1762 to 2011, but it is relatively complete only for the last 30 years. The number of landslides triggered by rainfall and earthquake are 157 and 123, respectively. The events are represented by points.

- Inventory of consequences. The purpose of this inventory was to quantify consequences in terms of number of persons killed by landslides. The source for this inventory was the DesInventar database (<http://www.desinventar.net/>). The consequences are aggregated at municipal level. For the purpose of this study, only events producing casualties were taken into account. The number of municipalities with casualties due to rainfall-induced landslides is 77, with 999 casualties distributed in 202 events. Regarding earthquake-induced landslides, casualties are reported only for 3 municipalities. Based on the historical evidence, the latter is clearly an underestimation, which is explained by the fact that consequences data for earthquake-induced landslides might be aggregated under the total consequences for earthquake events. This source of underestimation in landslide inventories has been previously acknowledged by Nadim et al. (2006).

Since the calibration of hazard in the bivariate and weights-of-evidence methods requires that the landslide events are represented by areas to enable the pixel-based regression, only the event-based inventories were used for adjusting the susceptibility and triggering factors in the aforementioned methods.

The historic inventory was used to adjust the boundaries between classes during the reclassification of hazard.

## 5 Results

### 5.1 Hazard

For the NGI method (see section 2.1 for description) four parameter rasters were used for evaluating susceptibility. Figure 18 illustrates an overlay of the input maps used in this method. These input rasters are multiplied by each other according to the expression in parenthesis on the right hand side in Eq. (1) and (2). The following rasters were used for the NGI method for deriving the susceptibility:

- Land cover.
- Slope.
- Accumulated rainfall over the wettest 5-month period.
- Lithology.

As a caution note, it should be remembered that the land cover maps are different for the earthquake and rainfall triggers, so two different susceptibility maps need to be obtained.

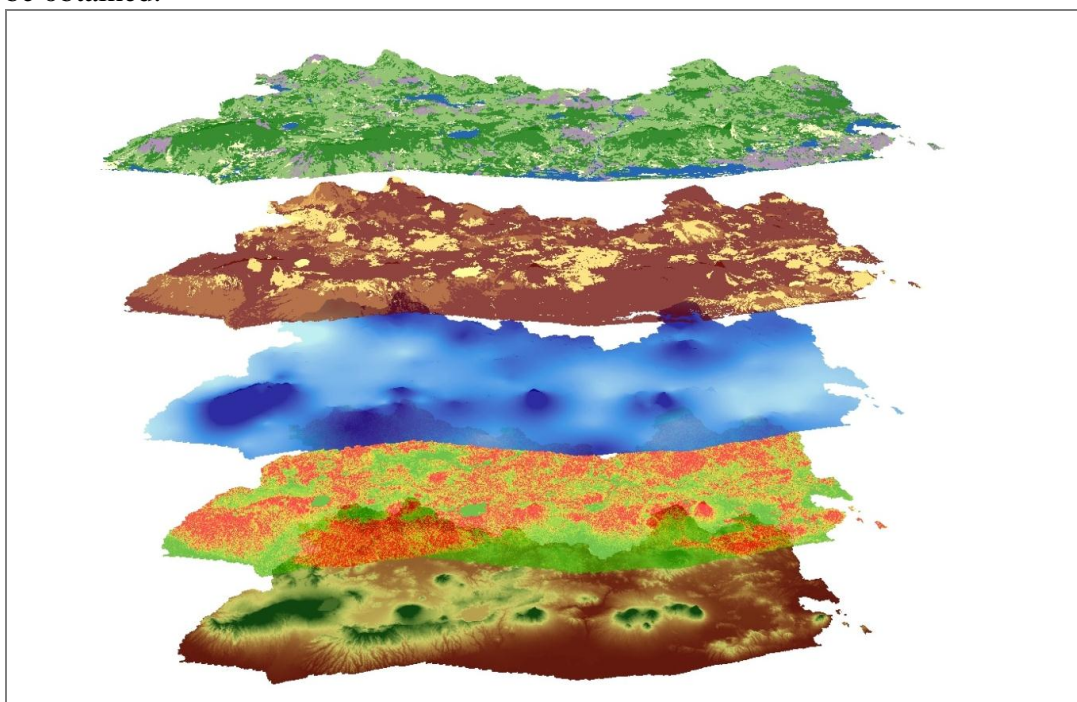


Figure 18. Illustration of parameters used for the NGI method.

In order to obtain hazard, the rainfall and earthquake triggers are multiplied with the susceptibility.

The resulting hazard maps for rainfall- and earthquake-induced landslides using the NGI method are presented in Figures 19 and 20.

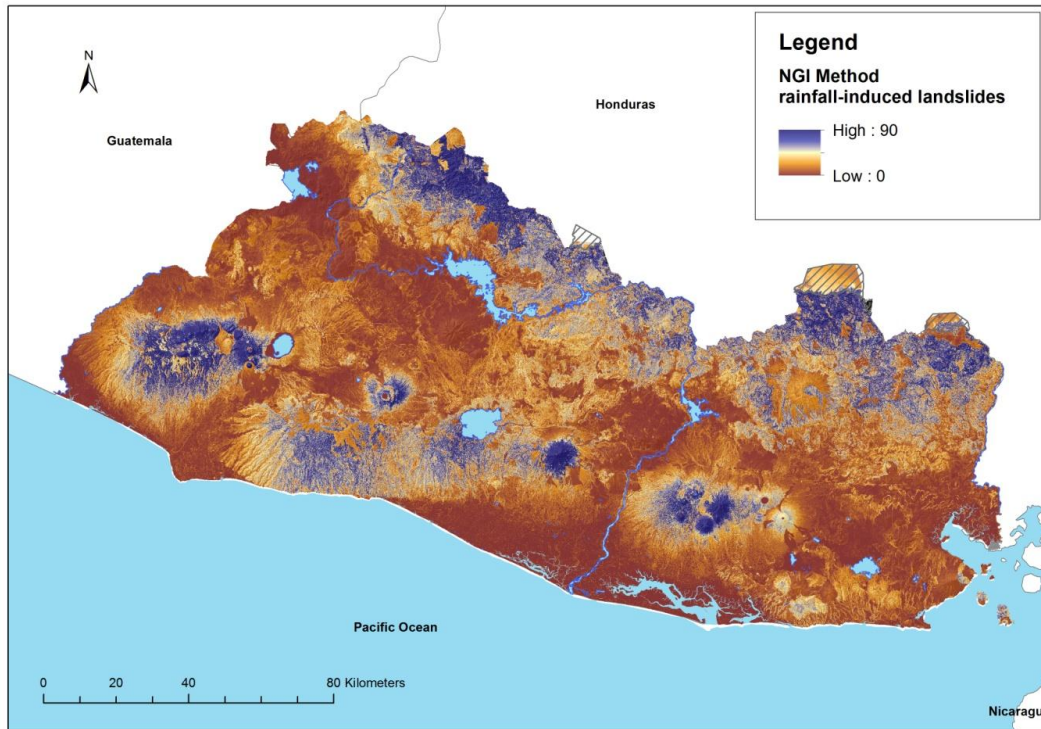


Figure 19. Hazard due to rainfall-induced landslides. NGI method.

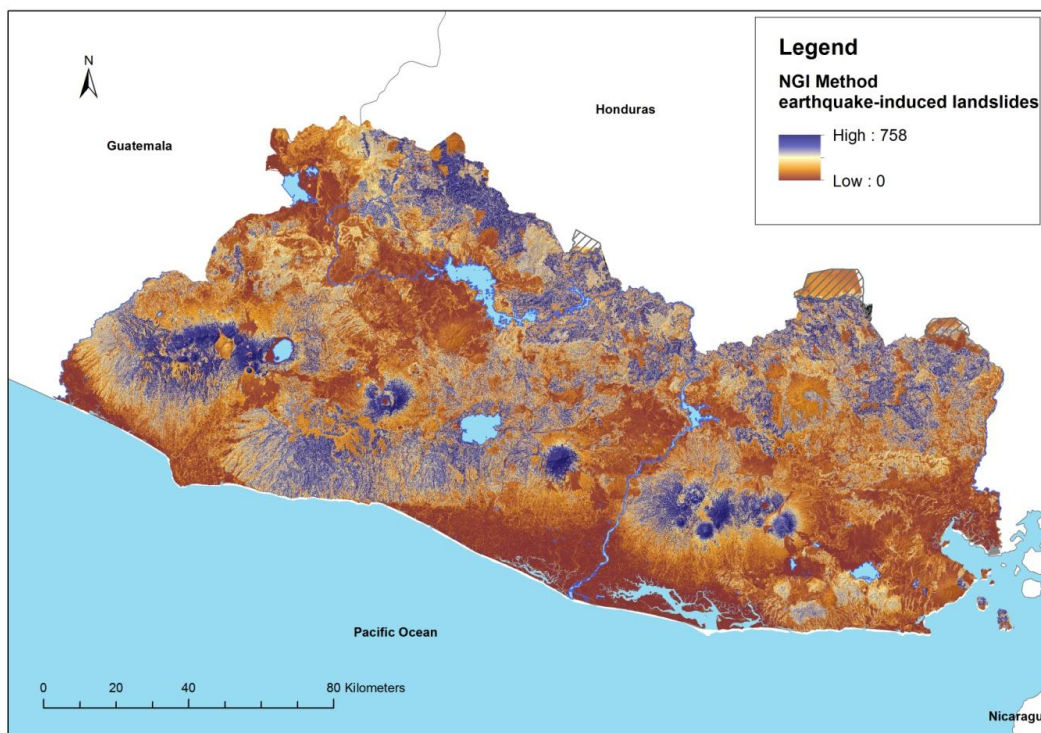


Figure 20. Hazard due to earthquake-induced landslides. NGI method.

For the evaluation of hazard using the bivariate and the weights-of-evidence methods (see descriptions in sections 2.2 and 2.3), the factor maps listed in Table 8 were used.

Table 8. Factors used for the bivariate method and weights-of-evidence method.

Factor map	Comment	
Aspect	Derived from DEM	Classified in North, North-East, etc.
Curvature plane		
Curvature profile		
Elevation		
Slope		
Landcover	58 landcover classes	
Lithology	27 lithology classes	
Moisture	Accumulated precipitation over the wettest 5-month period	
Road network	All orders (1 to 4) involved, buffered in 10 m steps	
Stream order	Strahler method	
PGA for 500-year return period	Trigger parameter for earthquake induced landslides	
Rainfall estimated as the maximum 1-day precipitation for a 10-year return period	Trigger parameter for rainfall induced landslides	

For obtaining the susceptible areas for the rainfall triggered landslides, the calculation areas were limited to the coverage of the aerial photos used for preparing the Hurricane Mitch inventory. For the assessment of the earthquake triggered landslides, the whole country was used for the calibration.

After applying the steps described in section 2.2 and using Eq. (3) to (7) with the datasets listed in Table 8, the resulting hazard maps are presented in Fig. 21 to 24.

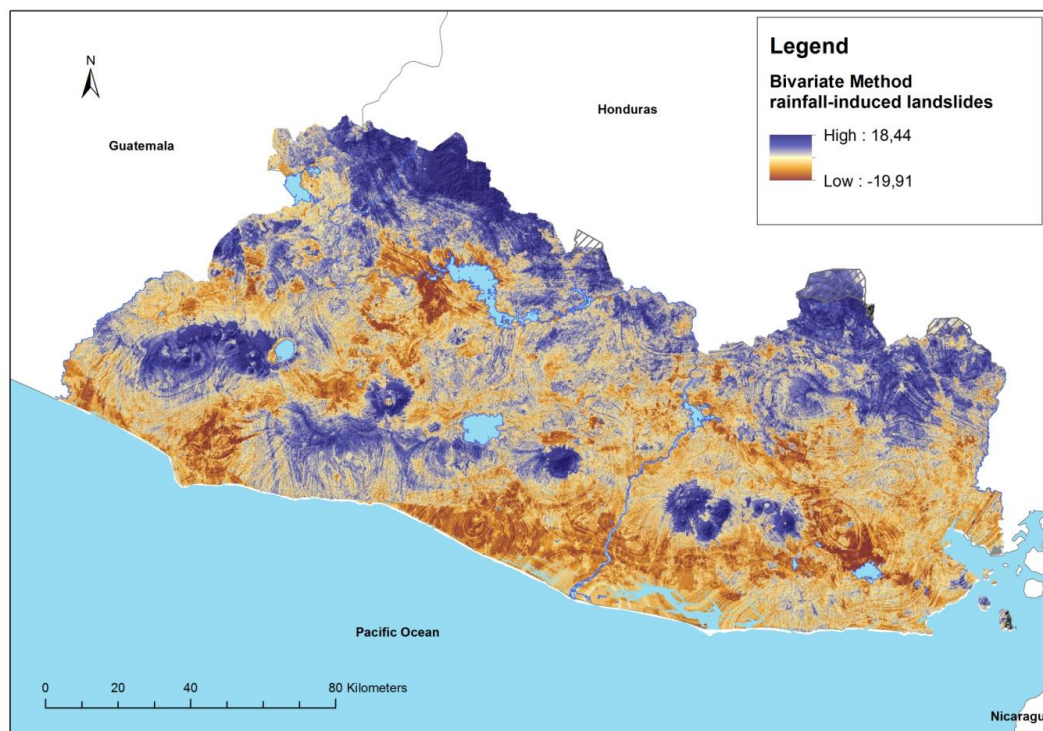


Figure 21. Hazard due to rainfall-induced landslides. Bivariate method.

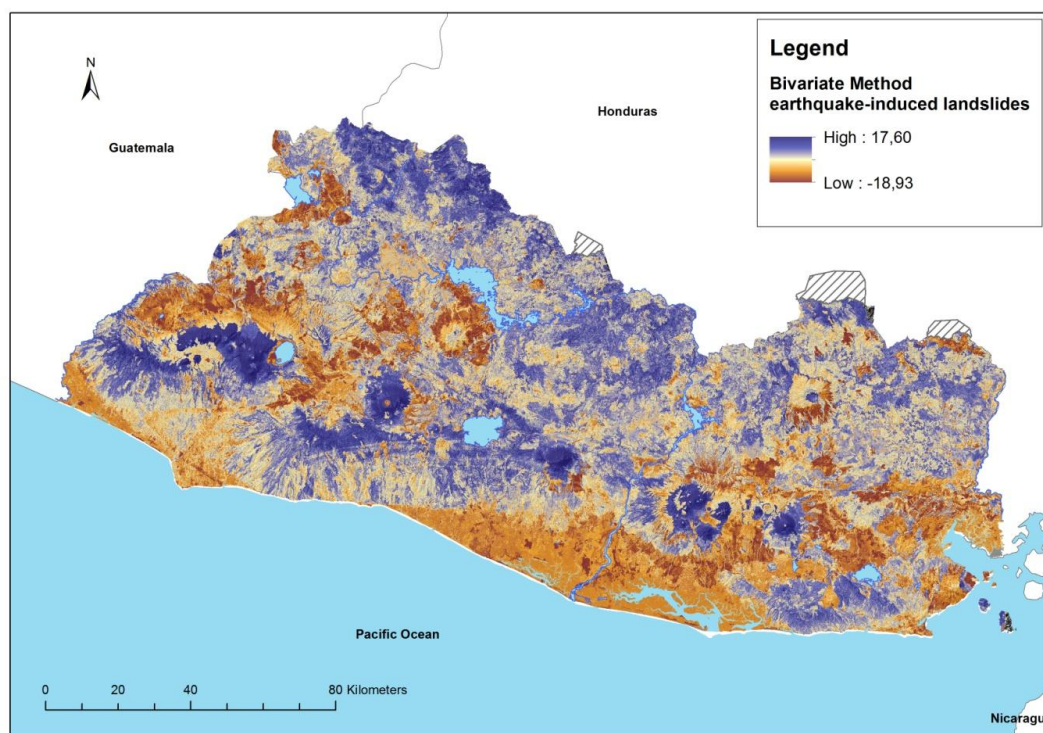


Figure 22. Hazard due to earthquake-induced landslides. Bivariate method.

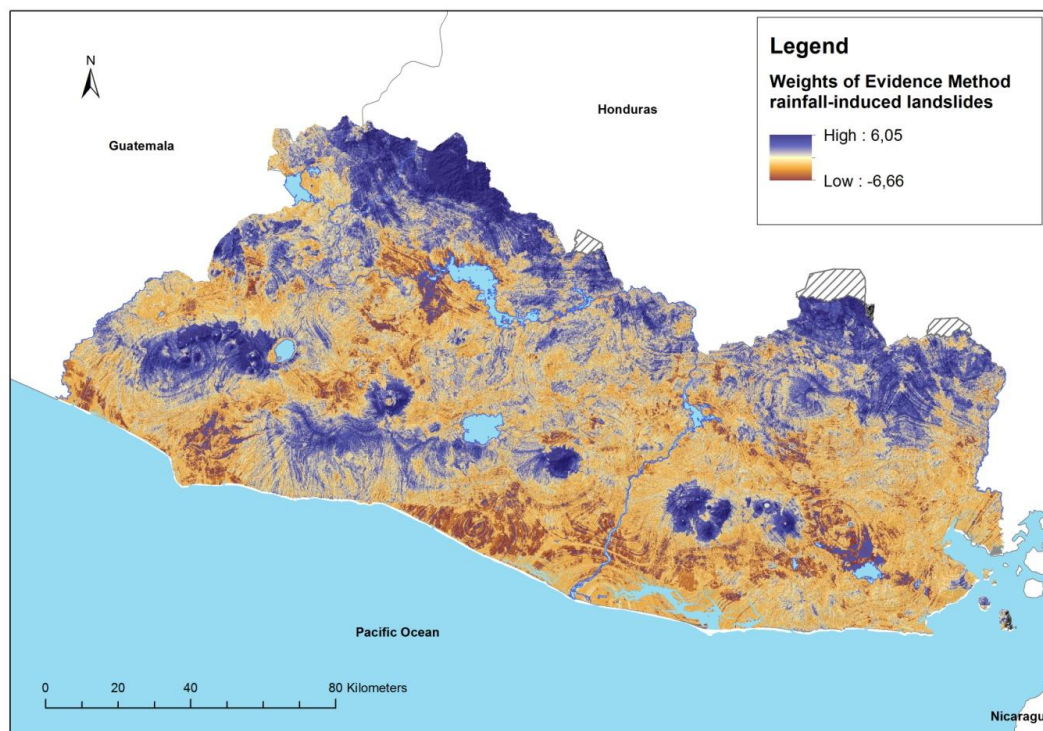


Figure 23. Hazard due to rainfall-induced landslides. Weights of evidence method.

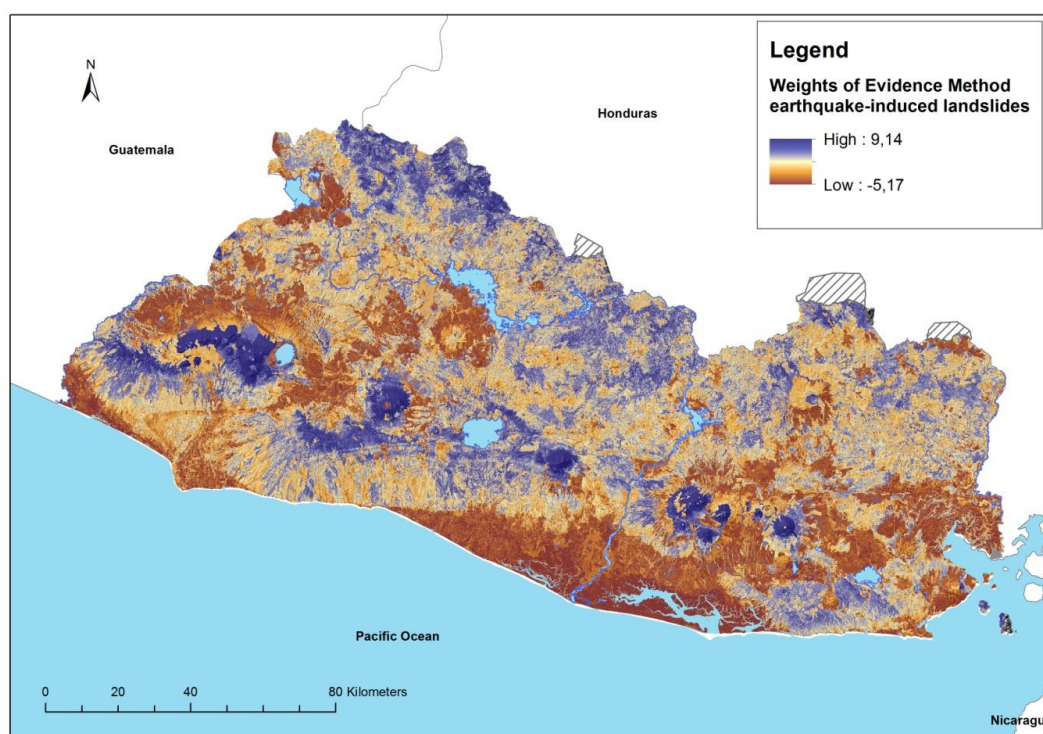


Figure 24. Hazard due to earthquake-induced landslides. Weights of evidence method.

Finally, the hazard maps that result from the NGI method, the bivariate method and the weights-of-evidence method are combined using Eq. (8) in section 2.4 and by setting  $w_k = 1/3$  (i.e., the three models are given the same priority), the hazard maps shown in Figures 25 and 26 are obtained. A reclassification was made using four classes: negligible, low, medium and high. Annual frequencies associated to each hazard class were estimated based on the historic inventory provided by DGOA. These frequencies are presented in Table 9.

Table 9. Hazard classes and annual frequencies estimated from the historic inventory provided by DGOA (see description of inventory in section 4.10).

Hazard class	Annual frequency per km <sup>2</sup> ( $1 \times 10^{-4}$ )
Negligible	< 1.8
Low	1.8 – 3.2
Medium	3.2 – 7.5
High	> 7.5

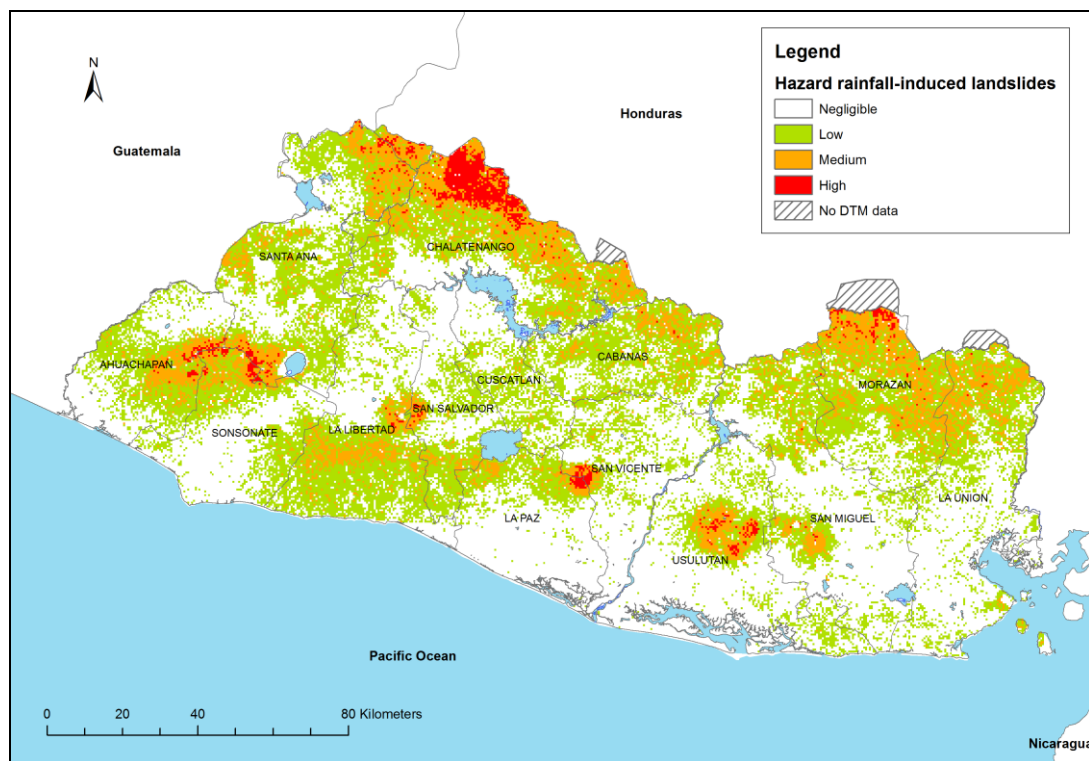


Figure 25. Hazard map for rainfall-induced landslides.

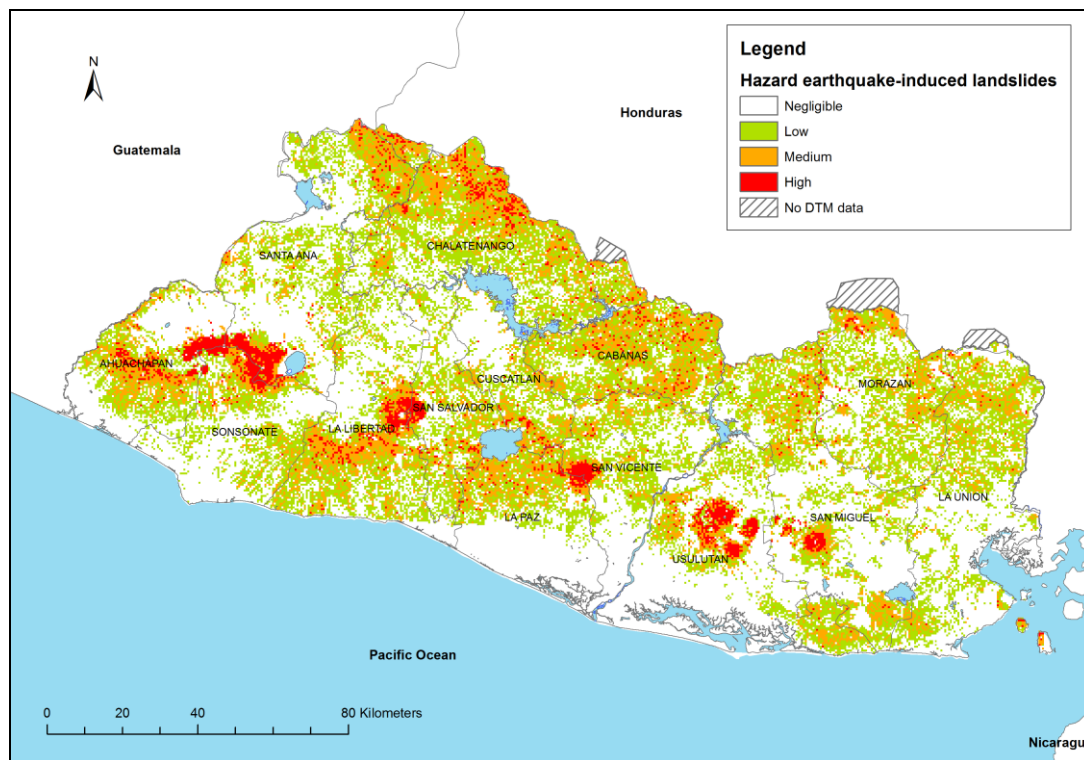


Figure 26. Hazard map for earthquake-induced landslides.

## 5.2 Exposure

Physical exposure was calculated as exposed population using the approach described in section 3.1 and the maps of population density (Fig. 16) and hazard (Fig. 25 and 26). The resulting exposure maps are presented in Figures 27 and 28.

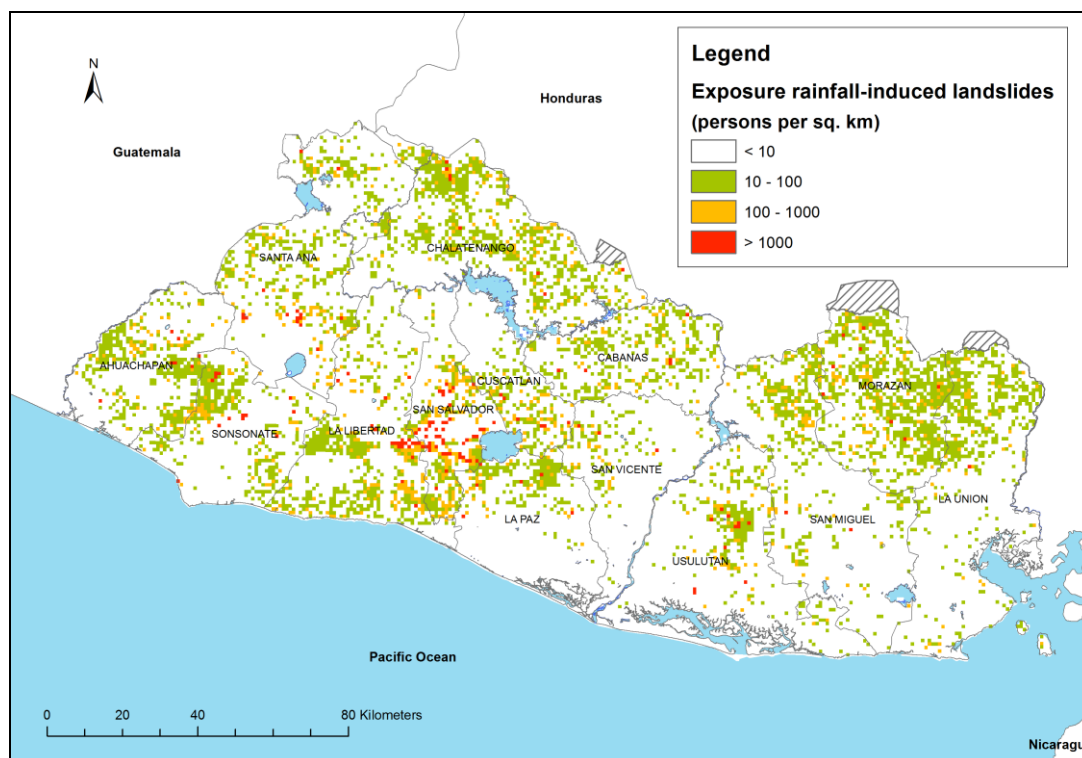


Figure 27. Population exposure to rainfall-induced landslides.

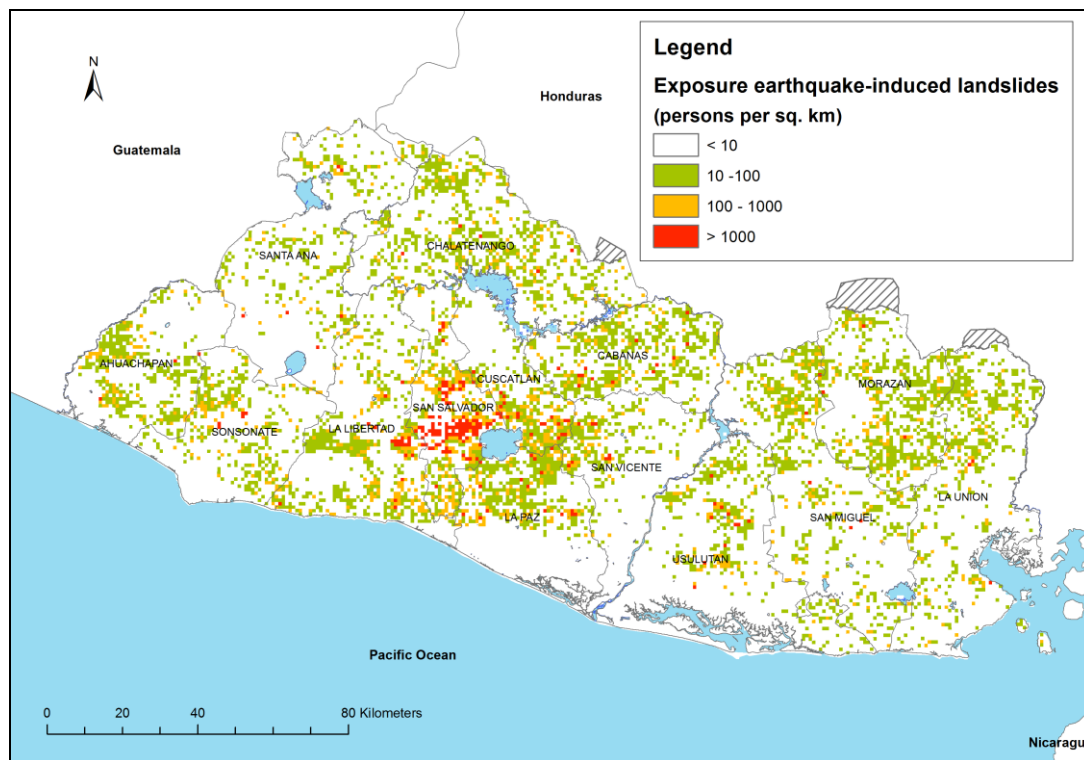


Figure 28. Population exposure to earthquake-induced landslides.

### 5.3 Risk

In the case of precipitation-induced landslides, risk was calibrated at municipal level using the corresponding exposure values, data from DesInventar (for estimating consequences), and Human Development Index (HDI) in the correlation function defined by Eq. (9). Consequences data were available for 76 of the 262 municipalities.

The calibration explained about 36% of the variation of the risk data, which indicates a low correlation. The correlation of each predictor with risk was as follows (the sign indicates whether the correlation is direct, “+” sign, or inverse, “-” sign):

- Physical exposure (+)
- Human Development Index (HDI) (+)

Hence, an increase in physical exposure and in Human Development Index leads to an increase in risk. For Human Development Index, this is unexpected since an improvement in the mean development level in an area (increase in HDI) normally should reduce the risk. In the case of El Salvador, this unexpected correlation between risk and HDI is, however, confirmed by historical observations. In September 1982, a single rainfall-induced debris flow initiated in the San Salvador volcano and caused 500 casualties in a neighbourhood in the municipality of Mejicanos, which has the 4<sup>th</sup> highest HDI in the country (0.826). This positive correlation between HDI and mortality risk was also obtained in Nepal and Sri Lanka in a previous assessment performed by NGI in South Asia. A possible explanation of this positive correlation is that all these countries (El Salvador, Nepal and Sri Lanka) experienced civil conflict in recent decades, which led to rapid, uncontrolled migration of people from rural to urban centres and taking up residence in hazardous areas.

The calibrated equation of landslide risk in El Salvador for precipitation-induced landslides is as follows:

$$\ln R_r = -5.48 + 0.206 \ln PE_r + 7.983 \ln \left( \frac{HDI_{SN}}{HDI_N} \right) \quad (10)$$

where  $R_r$  is the mortality risk (fatalities per year) due to precipitation-induced landslides,  $PE_r$  is physical exposure, and the term in parentheses is a transformed and normalised value of Human Development Index. The equation is only applicable to risk estimation at municipal level. Figure 29 presents the surface that corresponds to the regression in Eq. (10) and the observations used for calibration.

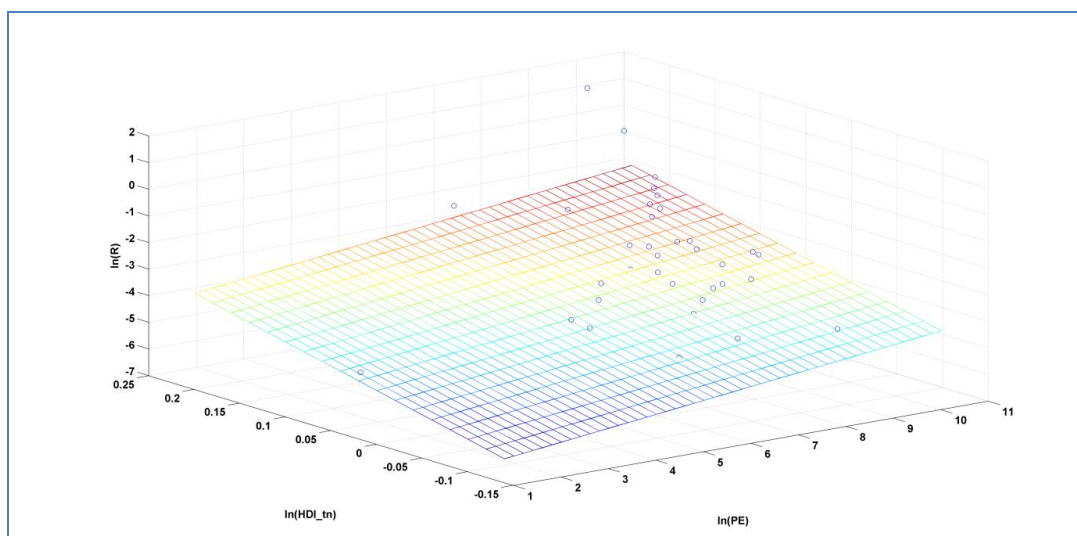


Figure 29. Risk model due to rainfall-induced landslides (plane representing Eq. 1) and observations (circle markers). PE is population exposure to rainfall-induced landslides, HDI\_tn is a transformed and normalised value of the Human Development Index, R is mortality risk in fatalities per year.

## 6 Discussion

The resulting hazard maps indicate much lower hazard due to earthquake-induced events than to rainfall-induced landslides in the northern part of the country. This difference is explained by the fact that seismic hazard is considerably higher on the south and central part of the country compared with the northern part. This is due to the proximity to the subduction zone to the south of the country and local systems of faults that run along the centre of the territory from west to east. These differences in seismicity control the spatial variation in landslide hazard when comparing the two types of triggering conditions.

Most of the country's population is settled in the three largest cities that lie along the central valleys that run from West to East. They are flanked by an active volcanic chain, which is in an ongoing mass wasting process in form of erosion and landslides due to the steep slopes and loose surface deposits. In particular, the Metropolitan Area of San Salvador, located at the centre of the country, concentrates about one third of the total population of 6 million.

In El Salvador, human development seems to be strongly correlated to the urban or rural nature of the settlements. The large urban centres in Santa Ana, San Salvador and San Miguel represent municipalities with high Human Development Index, HDI, which reaches a maximum of 0.88 in Antiguo Cuscatlán, one of the municipalities of the Metropolitan Area of San Salvador. The municipalities with the lowest HDI are mostly located to the north of the country, where rural settlements are abundant in areas that were strongly affected by a 12-year Civil war that ended two decades ago. The minimum HDI in the country is 0.56. Most of the

municipalities with the lowest HDI are in the Departments of Morazán and Cabañas.

Regarding population exposure, the main difference between the two types of triggering conditions is the lower exposure along the north of the country for earthquake-induced conditions than the corresponding to rainfall-triggered landslides. This is an obvious consequence of the differences in hazard distribution previously explained.

The calibrated risk model for rainfall-induced landslides was considered to have a too low correlation for estimating risk at municipal level. Therefore, it is recommended as an alternative that the exposure maps be used as a proxy for risk.

The calibration of risk for earthquake-induced landslides was not possible due to the lack of consequences data for a meaningful statistical analysis (consequences data available for only 3 municipalities). This is due to the fact that the consequences for this category of landslides are often reported as caused directly by the earthquake shaking, and not by earthquake-induced landslides.

The results of the present study can serve as a basis for detailed evaluations in those areas that are identified as critical in terms of hazard level and/or exposure. Since the hazard methods and scale that were herein applied allow identifying only the areas of potential initiation, further evaluations should also assess the potential for landslide propagation, which can be significant, particularly for rainfall-induced landslides. As an illustration, Figure 30 presents the simulations performed in a previous NGI research project in an area impacted by a debris flow that produced ~300 casualties. These evaluations require a careful assessment of the expected released volumes based on the local geomorphologic conditions and on experience gained from past events (both historical and pre-historical).

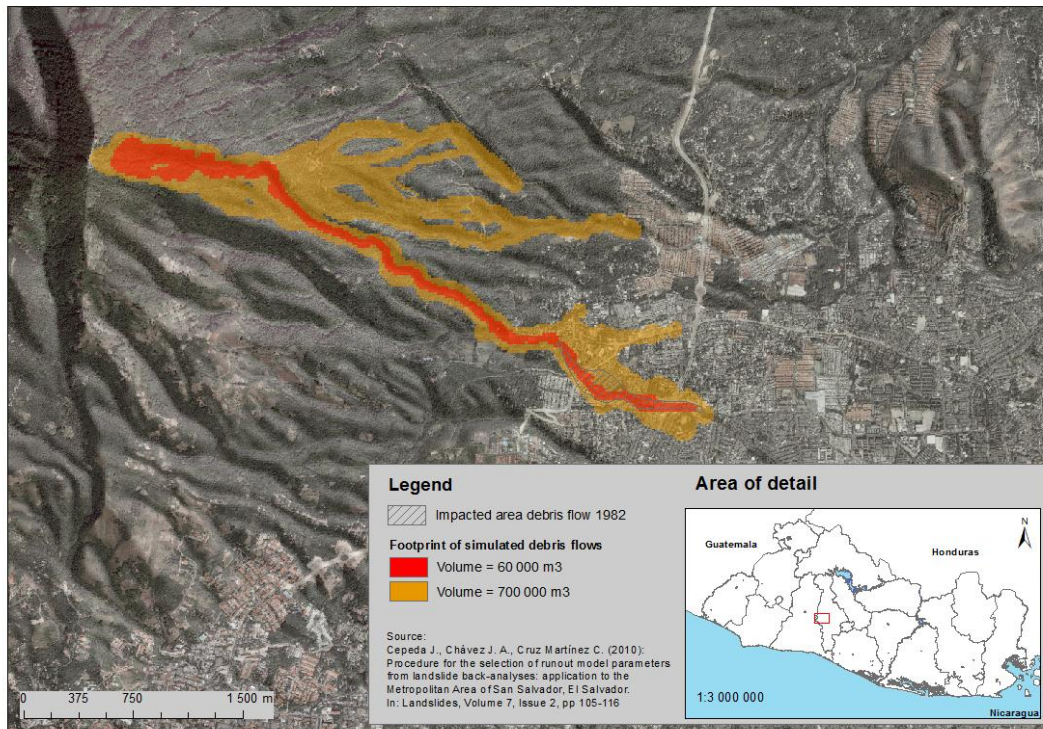


Figure 30. Results of numerical simulation of debris flows to the NW of the Metropolitan Area of San Salvador. The simulations were performed in an NGI research project (Cepeda et al., 2010a).

## 7 References

- Benito, B., Cepeda, J., and Diaz, J.M. (2004) Analysis of the spatial and temporal distribution of the 2001 earthquakes in El Salvador. Geological Society of America. Special Paper 375:339-356. <http://dx.doi.org/10.1130/0-8137-2375-2.339>
- Cepeda, J. (2009) Characterisation and risk management of rainfall-induced landslides. PhD dissertation, University of Oslo. <http://ask.bibsys.no/ask/action/show?pid=093394594&kid=biblio>
- Cepeda J., Benito M.B., Burgos E.A. (2004) Strong-motion characteristics of January and February 2001 earthquakes in El Salvador. Geological Society of America. Special Paper 375:405-421. <http://dx.doi.org/10.1130/0-8137-2375-2.405>
- Cepeda, J., Chávez, J.A., and Cruz Martínez, C. (2010a) Procedure for the selection of runout model parameters from landslide back-analyses: application to the Metropolitan Area of San Salvador, El Salvador. Landslides, 7(2), 105-116. <http://dx.doi.org/10.1007/s10346-010-0197-9>
- Cepeda, J., Smebye, H., Vangelsten, B., Nadim, F. and Muslim, D. (2010b) Landslide risk in Indonesia. Background paper prepared for the 2011 Global Assessment Report on Disaster Risk Reduction. Prepared by the International Centre for Geohazards, Norwegian Geotechnical Institute. Geneva, Switzerland: UNISDR. [http://www.preventionweb.net/english/hyogo/gar/2011/en/bgdocs/Cepeda\\_et\\_al.\\_2010.pdf](http://www.preventionweb.net/english/hyogo/gar/2011/en/bgdocs/Cepeda_et_al._2010.pdf)
- Crone, A.J., Baum, R.L., Lidke, D.J., Sather, D.N., Bradley, L.A., and Tarr, A.C. (2001) Landslides induced by hurricane Mitch in El Salvador: An inventory and descriptions of selected features. US Department of the Interior, US Geological Survey. [http://pdf.usaid.gov/pdf\\_docs/pnacr105.pdf](http://pdf.usaid.gov/pdf_docs/pnacr105.pdf)
- García-Rodríguez, M.J., Malpica, J.A., Benito, B., and Díaz, M. (2008) Susceptibility assessment of earthquake-triggered landslides in El Salvador using logistic regression. Geomorphology, 95(3), 172-191. <http://dx.doi.org/10.1016/j.geomorph.2007.06.001>
- Jaedicke, C.J., Sverdrup-Thygeson, K., Smebye, H., Syre, E., Vangelsten, B.V., Nadim, F., and Kalsnes, B. (2010) Identification of landslide hazard and risk “hotspots” in Europe. Deliverable D2.10, Work Package 2.4, SafeLand Project, 7th Framework Programme. <http://www.safeland-fp7.eu/results/Documents/D2.10.pdf>

- Marroquín, G., and Benito, B. (2009) Evaluación de la amenaza sísmica en El Salvador. Ministerio del Medio Ambiente y Recursos Naturales (El Salvador) and Technical University of Madrid (Spain), 176 pp.
- Mora C., S., and Vahrson, W. G. (1994). Macrozonation methodology for landslide hazard determination. Bulletin-Association of Engineering Geologists, 31(1): 49–58.
- Nadim, F., Kjekstad, O., Peduzzi, P., Herold, C. and Jaedicke, C. (2006). Global landslide and avalanche hotspots. Landslides, Vol. 3, No. 2, 159-174. <http://dx.doi.org/10.1007/s10346-006-0036-1>
- Kakiuchi, H (?) Study for establishment of national basic geographic data in the Republic of El Salvador. Chapter 2-4, p. 84-86. [http://www.mlit.go.jp/sogoseisaku/inter\\_e/project/technology/pdf/geographic\\_sys\\_e\\_02\\_04.pdf](http://www.mlit.go.jp/sogoseisaku/inter_e/project/technology/pdf/geographic_sys_e_02_04.pdf)
- Norwegian Geotechnical Institute (2009) Risk assessment and mitigation measures for natural- and conflict-related hazards in Asia-Pacific. [http://www.preventionweb.net/files/10455\\_OCHANGINaturalconflictrelated\\_hazard.pdf](http://www.preventionweb.net/files/10455_OCHANGINaturalconflictrelated_hazard.pdf)
- UNDP and FUNDAUNGO (2009) Almanaque 262. Estado del desarrollo humano en los municipios de El Salvador 2009. United Nations Development Programme – UNDP - and Fundación Dr. Guillermo Manuel Ungo – FUNDAUNGO, 314 pp.
- Smebye, H., and Kalsnes, B. (2009) Landslides. Appendix 1, section 4 in Global Assessment Report – GAR 2009. <http://www.preventionweb.net/english/hyogo/gar/appendices/documents/Appendix-1.doc>
- van Westen, C.J. (1997) Statistical landslide hazard analysis. ILWIS, 2, 73-84.
- van Westen, C.J. (2002) Use of weights of evidence modelling for landslide susceptibility mapping. ITC, Netherlands, 21 p.
- Vangelsten, B.V., and Smebye, H.C. (2010) Natural Disaster Risk Reduction Strategy in South Asia. Main report. NGI document no. 20091739-00-10-R.

# Kontroll- og referanseside/ Review and reference page



<b>Dokumentinformasjon/Document information</b>					
<b>Dokumenttittel/Document title</b> Landslide Hazard and Risk Assessment in El Salvador				<b>Dokument nr./Document No.</b> 20120052-01-R	
<b>Dokumenttype/Type of document</b> Report		<b>Distribusjon/Distribution</b> Limited		<b>Dato/Date</b> 14 December 2012	
				<b>Rev.nr.&amp;dato/Rev.No&amp;date.</b> 0	
<b>Oppdragsgiver/Client</b> The United Nations Office for Disaster Risk Reduction – UNISDR					
<b>Emneord/Keywords</b> Landslides, disaster risk, hazard mapping, risk mapping					
<b>Stedfesting/Geographical information</b>					
<b>Land, fylke/Country, County</b> El Salvador				<b>Havområde/Offshore area</b>	
<b>Kommune/Municipality</b>				<b>Felt navn/Field name</b>	
<b>Sted/Location</b>				<b>Sted/Location</b>	
<b>Kartblad/Map</b>				<b>Felt, blokknr./Field, Block No.</b>	
<b>UTM-koordinater/UTM-coordinates</b>					
<b>Dokumentkontroll/Document control</b>					
<b>Kvalitetssikring i henhold til/Quality assurance according to NS-EN ISO9001</b>					
Rev./ Rev.	Revisjonsgrunnlag/Reason for revision	Egen- kontroll/ Self review av/by:	Sidemanns- kontroll/ Colleague review av/by:	Uavhengig kontroll/ Independent review av/by:	Tverrfaglig kontroll/ Inter- disciplinary review av/by:
0	Original document	JMC	FNa		
		BaS			
<b>Dokument godkjent for utsendelse/ Document approved for release</b>		<b>Dato/Date</b> 14 December 2012		<b>Sign. Prosjektleder/Project Manager</b> Farrokh Nadim	

NGI (Norges Geotekniske Institutt) er et internasjonalt ledende senter for forskning og rådgivning innen geofagene. Vi utvikler optimale løsninger for samfunnet, og tilbyr ekspertise om jord, berg og snø og deres påvirkning på miljøet, konstruksjoner og anlegg.

Vi arbeider i følgende markeder: olje, gass og energi, bygg, anlegg og samferdsel, naturskade og miljøteknologi. NGI er en privat stiftelse med kontor og laboratorier i Oslo, avdelingskontor i Trondheim og datterselskap i Houston, Texas, USA.

NGI ble utnevnt til "Senter for fremragende forskning" (SFF) i 2002 og leder "International Centre for Geohazards" (ICG).

[www.ngi.no](http://www.ngi.no)

NGI (Norwegian Geotechnical Institute) is a leading international centre for research and consulting in the geosciences. NGI develops optimum solutions for society, and offers expertise on the behaviour of soil, rock and snow and their interaction with the natural and built environment.

NGI works within the oil, gas and energy, building and construction, transportation, natural hazards and environment sectors. NGI is a private foundation with office and laboratory in Oslo, branch office in Trondheim and daughter company in Houston, Texas, USA.

NGI was awarded Centre of Excellence status in 2002 and leads the International Centre for Geohazards (ICG).

[www.ngi.no](http://www.ngi.no)



Hovedkontor/Main office:  
PO Box 3930 Ullevål Stadion  
NO-0806 Oslo  
Norway

Besøksadresse/Street address:  
Sognsveien 72, NO-0855 Oslo

Avd Trondheim/Trondheim office:  
PO Box 1230 Sluppen  
NO-7462 Trondheim  
Norway

Besøksadresse/Street address:  
Pirsenteret, Havnegata 9, NO-7010 Trondheim

T: (+47) 22 02 30 00  
F: (+47) 22 23 04 48

[ngi@ngi.no](mailto:ngi@ngi.no)  
[www.ngi.no](http://www.ngi.no)

Kontonr 5096 05 01281 /IBAN NO26 5096 0501 281  
Org. nr./Company No.: 958 254 318 MVA

BSI EN ISO 9001  
Sertifisert av/Certified by BSI, Reg. No. FS 32989